

Latent Diffusion Model-Enabled Real-Time Semantic Communication Considering Semantic Ambiguities and Channel Noises

Jianhua Pei, *Student Member, IEEE*, Cheng Feng, *Student Member, IEEE*, Ping Wang, *Fellow, IEEE*, Hina Tabassum, *Senior Member, IEEE*, and Dongyuan Shi, *Senior Member, IEEE*

Abstract—Semantic communication (SemCom) has emerged as a new paradigm for 6G communication, with deep learning (DL) models being one of the key drives to shift from the accuracy of bit/symbol to the semantics and pragmatics of data. Nevertheless, DL-based SemCom systems often face performance bottlenecks due to overfitting, poor generalization, and sensitivity to outliers. Furthermore, the varying-fading gains and noises with uncertain signal-to-noise ratios (SNRs) commonly present in wireless channels usually restrict the accuracy of semantic information transmission. Consequently, this paper constructs a latent diffusion model-enabled SemCom system, and proposes three improvements compared to existing works: i) To handle potential outliers in the source data, semantic errors obtained by projected gradient descent based on the vulnerabilities of DL models, are utilized to update the parameters and obtain an outlier-robust encoder. ii) A lightweight single-layer latent space transformation adapter completes one-shot learning at the transmitter and is placed before the decoder at the receiver, enabling adaptation for out-of-distribution data and enhancing human-perceptual quality. iii) An end-to-end consistency distillation (EECD) strategy is used to distill the diffusion models trained in latent space, enabling deterministic single or few-step real-time denoising in various noisy channels while maintaining high semantic quality. Extensive numerical experiments across different datasets demonstrate the superiority of the proposed SemCom system, consistently proving its robustness to outliers, the capability to transmit data with unknown distributions, and the ability to perform real-time channel denoising tasks while preserving high human perceptual quality, outperforming the existing denoising approaches in semantic metrics.

Index Terms—Semantic communication, latent diffusion model, GAN inversion, channel denoising, semantic ambiguity.

I. INTRODUCTION

WITH the booming development of artificial intelligence (AI), augmented and virtual reality [1], 4K/6K streaming [2], and intelligent sensing devices for smart grids [3] and vehicles [4] within the Internet of things (IoT), an efficient and reliable communication system becomes an essential component in the realm of 6-th generation (6G) communications [5]. In information and communication technology, joint source-channel coding (JSCC) [6], [7] is committed to the integrated design of source and channel codes for efficient transmission of data, leveraging Shannon information theory. However, classic JSCC techniques, employing coding methods for engineering applications such as WebP [8], JPEG [9], JPEG2000 [10], and BPG [11], have solely focused on the statistical characteristics of the data being transmitted, disregarding the semantic content they encompass.

Recently, the pursuit of more efficient and intelligent data transmission has given rise to semantic communication (SemCom) systems [12], where the focus has shifted from traditional bit-level accuracy to the conveyance of meaning and intent. The essence of SemCom lies in its capacity to prioritize the transmission of essential information, thus promising significant improvements in bandwidth utilization and overall communication efficiency [13]. Fortunately, with the rapid advancement of machine learning, deep learning (DL) based SemComs have emerged as an important approach for the implementation of SemComs [14]. Specifically, SemCom built upon neural networks such as variational autoencoder (VAE) [15], residual network (ResNet) [16], convolutional neural network (CNN) [17], long short-term memory (LSTM) network [18], generative adversarial network (GAN) [19], and Transformer [14] have demonstrated effectiveness in extracting the semantic features of source data. This allows for the mapping of source data into a lower-dimensional space for transmission over noisy wireless channels to the receiver, where it can ultimately be decoded back into its original form, whether that be images [20], audio [21], text [14], or multimodal data [22]. Nonetheless, the intrinsic complexity of semantic information, coupled with the unpredictable nature of communication channels, poses new challenges that those SemCom systems are not designed to handle.

Currently, diffusion models (DMs) have taken the forefront in the field of AI-generated content (AIGC) and have achieved remarkable and landmark advancements [23], [24], surpassing other generative models. Consequently, the application of DMs to tackle challenges within SemCom systems is beginning to gain attraction [25]. Conditional DM, guided by semantic and free-space information from other users, progressively generate matching data for mixed visual reality applications [26]. Similarly, conditional DMs, guided by invertible neural networks [27], compressed one-hot maps [28], decoded low-quality data [29], and scene graphs [30], have been proposed for image transmission to achieve higher perceptual quality. DMs have also been adapted to rectify errors caused by channels with varying-fading gains and low signal-to-noise ratio (SNR) noises [31]. Wireless channel estimation has also been performed by complex architectures based on DMs [32], [33], whose practicality issues due to high complexity remain to be addressed. Besides serving as decoders for JSCC, DMs can also act as denoisers placed after decoders to enhance data quality [34]. In [35] and [36], prompts, latent embeddings, or noisy data are transmitted over wireless channels

to the receiver as starting points or input conditions for DMs, inevitably increasing bandwidth burden. However, the primary bottleneck of DMs lies in their slow data generation speed due to the multi-step prediction process required to improve reconstruction quality, making such time-consuming communication impractical for real-time SemCom and edge users. Thus, some denoising or encoding methods opt for latent DM (LDM) [37] or acceleration techniques [38], [39] to significantly reduce the computational complexity. Nevertheless, since these enhanced approaches still feature a multi-step process during sampling, they inadequately address the challenges of real-time SemCom.

DMs-based SemCom offers high perceptual quality but also introduces a bottleneck of high latency. Moreover, structural errors, noises, and data following unknown distributions can introduce inaccuracies and distortions in the transmitted information when DL-based SemCom systems are deployed. The former, known as semantic errors [40], can arise from exploiting the vulnerabilities of DL models by adversarial attacks that lead to semantic discrepancies. Additionally, when a DL-based SemCom system trained by the specific category of data transmits out-of-distribution data [19], [41], the reconstructed data at the receiver may also be semantically ambiguous due to the prevalent issues of poor generalization and overfitting in current AI models. To balance sampling quality with speed, LDMs have been chosen as the underlying architecture for the SemCom approach. In summary, while LDMs excel at abstracting and encoding semantic content, the transmission process remains susceptible to semantic ambiguities from semantic errors or out-of-distribution data, i.e., misinterpretations of the meaning or intention behind the transmitted data and channel noises under different conditions.

To address these issues, this paper presents a comprehensive framework that enhances real-time SemCom by leveraging the capabilities of LDMs while simultaneously considering the effects of semantic ambiguities and channel imperfections. The proposed SemCom model builds upon and enhances the foundational architecture of a pretrained Wasserstein GAN [42] with VAE (VAE-WGAN). The overall contribution of this approach is threefold:

- 1) Semantic errors can significantly disrupt the normal encoding and decoding of DL-based JSCC systems. To address this, the vulnerabilities of the pretrained encoder and generator are exploited using convex optimization to determine the most significant undetectable semantic errors. The pretrained encoder is then updated with the obtained semantic errors to refine the neural network parameters, making the encoder robust and resilient to anomalously transmitted data. This parameter update process with data augmentation is self-supervised.
- 2) A rapid domain adaptation strategy is introduced to ensure the reconstructed data is semantically accurate at the receiver when the SemCom system transmits data with an unknown distribution. This strategy employs two additional lightweight single-layer neural networks that perform on-line one-shot or few-shot learning based on adversarial learning strategies. The updated parameters are transmitted to the dynamic neural network deployed at the receiver

through the shared knowledge [12] of the SemCom system, while the parameters of other networks remain unchanged, thus achieving low-cost latent space transformation.

- 3) Inspired by channel denoising DMs [37] and consistency distillation [43], the LDM based on ordinary differential equation (ODE) trajectories and variance explosion strategy is trained with known channel state information (CSI) [32], [33]. During the sampling phase, it can denoise the received equalized signals according to different CSIs. Furthermore, the end-to-end consistency distillation (EECD) approach that considers semantic metrics is proposed to distill the trained LDM, ultimately transforming the multi-step denoising process into a deterministic one-step real-time denoising procedure, capable of flexibly addressing varying fading channels and uncertain SNRs.

The efficiency and reliability of the proposed SemCom system in term of perceptual quality and timeliness are validated by rigorous and extensive experiments, providing concrete evidence of its superiority over conventional methods.

The rest of this paper is organized as follows. Section II briefly introduces the proposed wireless SemCom system model and existing challenges. Section III elaborates on the JSCC design of the proposed SemCom system for transmitting data with unknown errors and distributions. The real-time channel denoising implementation is established by EECD in Section IV. Numerical experiments are given in Section V. Section VI concludes the paper. Supporting lemmas are included in the Appendix for reference.

II. SYSTEM MODEL AND PROBLEM FORMULATION

The proposed SemCom system model depicted in Fig. 1 consists of the encoder $E_\phi(\cdot)$ for semantic encoding with target distribution $q_\phi(z|\mathbf{x})$ at the transmitter, DM $\epsilon_\theta(\cdot, \cdot)$ with denoised latent vector's distribution $p_\theta(z)$ at the receiver, and decoder $G_\psi(\cdot)$ for semantic decoding with reconstruction target distribution $q_\psi(\mathbf{x}|z)$ by utilizing the synthesized encodings z from DM. The goal of training this LDM is to learn $\{\phi, \theta, \psi\}$ by minimizing the overall variational upper bound [44], defined as follows:

$$\begin{aligned}
 \mathcal{L}_{JSCC}(\phi, \theta, \psi) &= \mathbb{E}_{q_\phi(z|\mathbf{x})} [\mathcal{D}_{KL}(q_\phi(z|\mathbf{x})||p_\theta(z))] + \mathbb{E}_{q_\phi(z|\mathbf{x})} [-\log q_\psi(\mathbf{x}|z)] \\
 &= \underbrace{\mathbb{E}_{q_\phi(z|\mathbf{x})} [\log q_\phi(z|\mathbf{x})]}_{\text{transmitter encoding entropy}} + \underbrace{\mathbb{E}_{q_\phi(z|\mathbf{x})} [-\log p_\theta(z)]}_{\text{channel cross entropy}} \\
 &\quad + \underbrace{\mathbb{E}_{q_\phi(z|\mathbf{x})} [-\log q_\psi(\mathbf{x}|z)]}_{\text{receiver reconstruction term}}, \tag{1}
 \end{aligned}$$

where $\mathcal{D}_{KL}(\cdot||\cdot)$ denotes the Kullback-Leibler divergence between two distributions, and $q_\phi(z|\mathbf{x})$ approximates the true posterior $q_\psi(z|\mathbf{x})$ of decoder. The loss in Eq. (1) has been widely applied and validated in fast data generation [45]. Unlike data generation, the goal of SemCom systems is to make the reconstructed data in receivers shows desired meaning. Consequently, Eq. (1) is divided into three terms: the encoding entropy term at the transmitter, the cross entropy term for synthesized denoised bottlenecks z at the wireless channel, and the reconstruction term at the receiver. However,

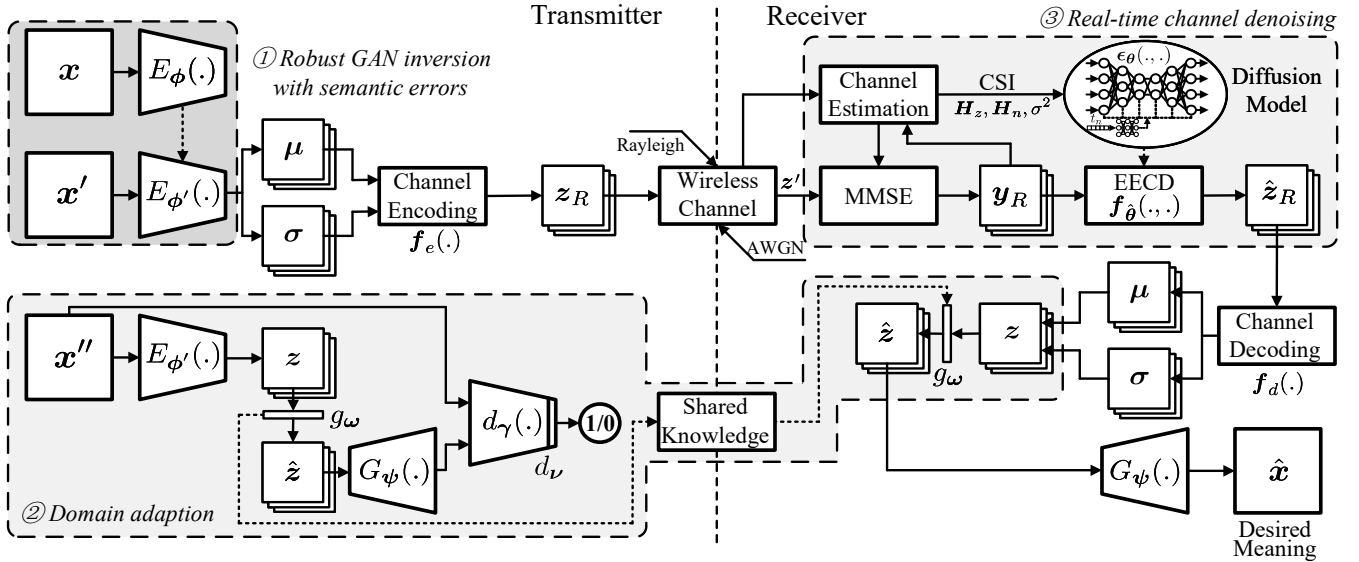


Fig. 1. The proposed semantic communication system model with three addressed deep learning-based communication challenges: ① robust GAN inversion with semantic errors, ② domain adaptation with unknown distribution, and ③ real-time wireless channel denoising with end-to-end consistency distillation.

as stated in Section I, the LDM-enabled SemCom system faces the following three major challenges:

1) Semantic Error: Due to unreasonable photographing, storage, or cyber attacks, the transmitted data may contain some imperceptible errors or noises, which may cause DL-based communication systems to reconstruct data with wrong semantics based on the contaminated data x' at the receiver. **2) Unknown Distribution:** When a DL-based communication system transmits data x'' with unknown distribution, i.e., the data type is not included in the training dataset, the decoder may generate data with different meaning. A lot of works on transfer learning are dedicated to address the challenge of domain adaptation [19], [41], [46], but strategies for quickly transmit out-of-distribution data still need further exploration. **3) Channel Uncertainties:** The wireless channels are inevitably subject to varying fading gains and noises with uncertain SNRs. For this reason, the received latent bottleneck is the data z' with noises and bit errors. DMs can utilize the cross entropy term $\mathbb{E}_{q_\phi(z|x)} [-\log p_\theta(z)]$ to solve the mapping $p(z|z')$, correct bit errors [31], or do joint channel estimation and denoising [32], [33], [37]. Nonetheless, these approaches still require uncertain multi-step evaluations to generate clean z , hindering the real-time implementation of SemCom systems. As a result, define x'/x'' as the transmitted data for aforementioned potential issues, the communication objective terms in Eq. (1) are rewritten as:

- Transmitter: $\mathbb{E}_{q_\phi(z|x'/x'')} [\log q_\phi(z|x'/x'')]$,
- Wireless channel: $\mathbb{E}_{q_\phi(z|x'/x'')} [-\log p_\theta(z|z')]$,
- Receiver: $\mathbb{E}_{q_\phi(z|x'/x'')} [-\log q_\psi(x/x''|z)]$.

The proposed SemCom system addresses the above three challenges of the DL-based communication system point-to-point. The basic encoder-decoder architecture of the proposed system consists of a variational encoder $E_\phi(\cdot)$ and generator $G_\psi(\cdot)$ of WGAN. The fundamental principles and joint training algorithm are detailed in Subsection III-A and Subsection III-B. As illustrated in Fig. 1, the threefold improvements are further clarified as follows:

1) Robust GAN Inversion: The imperceptible semantic error that leads to the maximum reconstruction error in the DL-based SemCom system is defined and obtained through adversarial convex optimization. Based on this semantic error, the parameters of the optimized robust encoder are updated from ϕ to ϕ' to encode normal latent space for transmission. The specific GAN robust inversion method is detailed in Subsection III-C. **2) Domain Adaptation:** When transmitting out-of-distribution data, the lightweight single-layer g_ω and d_ν are exploited for one-shot fast and adversarial domain adaptation learning. The learned parameters ω will be seamlessly transmitted to the receiver along with the data for latent space transformation, and the decoder will ultimately output semantically consistent data. The specific implementation can be found in Subsection III-D. **3) Real-time Channel Denoising:** Assuming that the CSIs are known, EECD is proposed to distill LDM from a multi-step denoising process into one setp, thereby reducing the computational complexity of online sampling process of DM during real-time communication. The detailed wireless channel modeling, training and sampling approaches of the latent channel denoising DM, and one-step real-time channel denoising algorithm are elucidated in Section IV.

III. DEEP JSCC FOR DATA WITH UNKNOWN ERRORS AND DISTRIBUTIONS

In this section, the selection of the encoder and decoder for the proposed robust and high-quality JSCC is further detailed. In Subsection III-A, WGAN and its higher quality variants are introduced to serve as the decoders for receivers. Subsection III-B firstly presents the joint training algorithm of VAE and WGAN, and Subsection III-C then provides an improved encoder that is robust to errors. The fast and reliable SemCom approach for data of unknown distribution is implemented in Subsection III-D by out-of-distribution latent space exploration.

A. Decoder: Wasserstein GAN and other variants

GANs with slightly lower generation quality than DMs are still selected as the decoder for the proposed LDM-enabled JSCC for its single-step data generation property. GAN is formulated based on zero-sum game between a discriminator $D_\gamma(\cdot)$ and a generator $G_\psi(\cdot)$ with the adversarial training objective

$$\min_{\psi} \max_{\gamma} \mathbb{E}_{\mathbf{x} \sim q(\mathbf{x})} [\log D_\gamma(\mathbf{x})] + \mathbb{E}_{\mathbf{z} \sim q_\psi(\mathbf{z})} [\log (1 - D_\gamma(G_\psi(\mathbf{z})))] \quad (2)$$

where $q_\psi(\mathbf{z})$ is the prior distribution of latent vector \mathbf{z} and $q_\psi(\mathbf{z}) = \mathcal{N}(\mathbf{0}, \mathbf{I})$ in GANs. Unfortunately, although GAN can generate higher quality data compared to other generative models such as VAE, it still faces some issues such as training instability and collapse mode. To overcome these challenges, WGAN [42] is established by replacing \mathcal{D}_{KL} and Jensen-Shannon divergence \mathcal{D}_{JS} with Wasserstein distance \mathcal{D}_W . In this way, the objective of WGAN can be decoupled as

$$\min_{\psi} \mathbb{E}_{\mathbf{z} \sim q_\psi(\mathbf{z})} [\mathcal{D}_W(\mathbf{x} \parallel G_\psi(\mathbf{z}))] \Leftrightarrow -\mathbb{E}_{\mathbf{z} \sim q_\psi(\mathbf{z})} [D_\gamma(G_\psi(\mathbf{z}))] \\ \min_{\gamma} -\mathbb{E}_{\mathbf{x} \sim q(\mathbf{x})} [D_\gamma(\mathbf{x})] + \mathbb{E}_{\mathbf{z} \sim q_\psi(\mathbf{z})} [D_\gamma(G_\psi(\mathbf{z}))]. \quad (3)$$

Furthermore, the variants of GAN that have been proposed for better perceptual reconstruction can also be utilized as the JSCC decoder. Among them, StyleGAN [47], Diff-GAN trained based on DMs [48], and Diff-Instuct GAN [49] distilled from DMs have achieved impressive generation results, and the latter two models are even comparable to the DMs in some datasets. Consequently, when receivers have higher requirements on decoding data quality, WGAN can be flexibly replaced with these superior variants, as they have the same architecture as the original GANs.

B. Encoder: GAN Inversion by VAE-WGAN

Compared to VAE, GANs are skilled in generating data with high-resolution. Nonetheless, the task of SemCom is to ensure that the signals received by receivers can accurately convey the meaning, while minimizing the bandwidth of SemCom. For this reason, JSCC requires an encoder to determine the latent bottlenecks of the transmitted data, also known as GAN inversion [50]. Commonly, the solution of GAN inversion is to utilize a neural network-based encoder to find the optimal latent vector \mathbf{z} given the transmitted data \mathbf{x} . Ignoring the channel's cross entropy term of the latent space and taking into account the receiver reconstruction term and the transmitter encoding entropy, the variational upper bound defined in Eq. 1 can be transformed into

$$\mathcal{L}'_{JSCC} = \mathbb{E}_{q_\phi(\mathbf{z}|\mathbf{x})} [-\log p_\psi(\mathbf{x}|\mathbf{z})] + \mathbb{E}_{q_\phi(\mathbf{z}|\mathbf{x})} [\log q_\phi(\mathbf{z}|\mathbf{x})] \\ \geq \mathbb{E}_{q_\psi(\mathbf{z})} [-\log p_\psi(\mathbf{x})] + \mathbb{E}_{q(\mathbf{x})} [\mathcal{D}_{KL}(q_\phi(\mathbf{z}|\mathbf{x}) \parallel p_\psi(\mathbf{z}|\mathbf{x}))] \\ \geq \mathbb{E}_{q_\psi(\mathbf{z})} [-\log p_\psi(\mathbf{x})], \quad (4)$$

where the proof can be seen in Appendix A. Apparently, the term $\mathbb{E}_{q_\psi(\mathbf{z})} [-\log p_\psi(\mathbf{x})]$ in Eq. (4) can be replaced with the training objective of the generator $G_\psi(\cdot)$ of WGAN, and term $\mathbb{E}_{q(\mathbf{x})} [\mathcal{D}_{KL}(q_\phi(\mathbf{z}|\mathbf{x}) \parallel p_\psi(\mathbf{z}|\mathbf{x}))]$ indicates that the

encoding latent vector \mathbf{z} should be as consistent as possible with the input latent space of generator $G_\psi(\cdot)$ under the same transmitted data \mathbf{x} . Like VAE, the output of encoder can be represented as $q_\phi(\mathbf{z}|\mathbf{x}) \sim \mathcal{N}(\boldsymbol{\mu}, \boldsymbol{\sigma}^2)$, and \mathbf{z} is reparameterized as $\mathbf{z} = \boldsymbol{\mu} + \boldsymbol{\sigma} \odot \boldsymbol{\epsilon}$, where $\boldsymbol{\epsilon} \sim \mathcal{N}(\mathbf{0}, \mathbf{I})$ and \odot denotes the element-wise product. Consequently, by combining the decoupled optimization objectives of WGAN and Eq. (4), the training process of deep CNN based VAE-WGAN can be found in [51].

C. Robust Encoder

As discussed in Section II, VAE-WGAN based SemCom systems suffer from inevitable vulnerabilities. The adversarial attack methods explore the vulnerabilities of neural networks utilized for classification and regression tasks, with the goal of determining a sufficiently small and unnoticed error δ to mislead the classification or regression results. The unified optimization objective of adversarial attacks is given by

$$\min_{\delta} \mathbf{d}(\mathbf{x}, \mathbf{x} + \delta) \\ \text{s.t.: } \mathbf{f}(\mathbf{x} + \delta) = \text{target}, \quad \mathbf{L} \leq \mathbf{x} + \delta \leq \mathbf{U}, \quad (5)$$

where $\mathbf{d}(\cdot, \cdot)$ is the distance function, $\mathbf{f}(\cdot)$ is the attacked neural network, *target* denotes the output of the DL model, \mathbf{L} and \mathbf{U} represent the physical lower and upper bounds of input data \mathbf{x} , respectively. Specifically, in classification tasks, *target* is the class that is inconsistent with original category of \mathbf{x} , e.g., the hackers can exploit objective (5) to make their cyber attacks undetectable by network $\mathbf{f}(\cdot)$. In regression tasks, *target* represents the output data that is not the same as the original regression results, e.g., when transmitting a digital image in SemCom systems, decoder may reconstruct another type of digital image with semantic ambiguities.

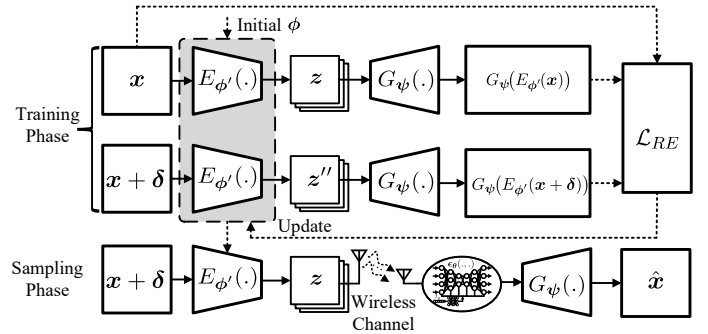


Fig. 2. Self-supervised robust encoder optimization with semantic error δ .

In order to address the challenges of semantic errors, SemCom systems should have a robust and enhanced encoder that can handle those outliers. The objective for the sufficiently small semantic error that leads to the maximum reconstruction error are given by

$$\max_{\delta} \mathbf{d}(G_\psi(E_\phi(\mathbf{x})), G_\psi(E_\phi(\mathbf{x} + \delta))) \\ \text{s.t.: } E_\phi(\mathbf{x} + \delta) \sim \mathcal{N}(\mathbf{0}, \mathbf{I}), \|\delta\|_p \leq \varepsilon, \mathbf{L} \leq \mathbf{x} + \delta \leq \mathbf{U}, \quad (6)$$

where $\|\cdot\|_p$ denotes the p-norm. In this way, objective (6) simultaneously utilizes the vulnerabilities of both the encoder

$E_\phi(\cdot)$ and generator $G_\psi(\cdot)$. When solving (6), its objective can be transformed into a standard convex optimization problem

$$\min_{\delta} \underbrace{\lambda \|\delta\|_p - \mathbf{d}(G_\psi(E_\phi(\mathbf{x})), G_\psi(E_\phi(\mathbf{x} + \delta)))}_{e(\delta)} \quad (7)$$

s.t.: $E_\phi(\mathbf{x} + \delta) \sim \mathcal{N}(\mathbf{0}, \mathbf{I}), \mathbf{L} \leq \mathbf{x} + \delta \leq \mathbf{U}$,

where λ is the penalty coefficient. The constrained convex optimization problem can be solved by using the projected gradient descent (PGD) [52] iterative optimization method to obtain semantic error δ . Consequently, the semantic error at the i -th iteration δ^i is denoted by

$$\delta^i = P_C(\delta^{i-1} - \eta \nabla_{\delta} e(\delta^{i-1})) = P_C(\zeta^i), \quad (8)$$

where $P_C(\zeta^i)$ represents the projection of $e(\delta)$ on the set of constraints C , i.e., $\delta^i = P_C(\zeta^i) := \arg \min_{\delta \in C} \frac{1}{2} \|\delta - \zeta^i\|_2^2$. Let \mathbf{z}'' be the erroneous latent vector encoded from data containing semantic errors $\mathbf{x}' = \mathbf{x} + \delta$, the robust variational upper bound (VUB) for semantic errors is defined as

$$\begin{aligned} \mathbb{E}_q[-\log p_\psi(\mathbf{x})] &= \mathbb{E}_q \left[-\log \int p_\psi(\mathbf{x}, \mathbf{x} + \delta) d(\mathbf{x} + \delta) \right] \\ &\leq \mathbb{E}_{q(\mathbf{z})} [-\log p_\psi(\mathbf{x}|\mathbf{z})] + \mathbb{E}_{q(\mathbf{z})} [-\log p_\psi(\mathbf{z})] \\ &+ \mathbb{E}_{q(\mathbf{z}'')} [-\log p_\psi(\mathbf{z}'')] + \frac{\beta}{2} \mathbb{E}_{q(\mathbf{z}, \mathbf{z}'')} \mathbf{d}(\mathbf{z}, \mathbf{z}'') \\ &- \mathbb{E}_{q(\mathbf{z}, \mathbf{z}'')} [-\log q(\mathbf{z}, \mathbf{z}'')], \end{aligned} \quad (9)$$

where the proof can be seen in Appendix B. Evidently, the first and second terms of Eq. (9) have been addressed in VAE-WGAN based JSCC, and the third term has also been optimized by sloving the semantic errors δ . For this reason, the training objective of robust encoder is

$$\min_{\phi'} \frac{\beta}{2} \mathbb{E}_{q(\mathbf{z}, \mathbf{z}'')} \mathbf{d}(\mathbf{z}, \mathbf{z}'') + \mathbb{E}_{q(\mathbf{z}, \mathbf{z}'')} [\log q(\mathbf{z}, \mathbf{z}'')], \quad (10)$$

where ϕ' denotes the robust encoder parameters. In [53], the objective (10) is equivalent to minimizing the Wasserstein distance between \mathbf{z} and the incorrect \mathbf{z}'' . Nevertheless, the ultimate goal of SemCom is to accurately reconstruct the transmitted data. Therefore, as the parameter ψ is fixed, the optimal robust encoder parameters ϕ' considering both encoder and decoder vulnerabilities is

$$\begin{aligned} \phi' = \arg \min_{\phi'} \mathcal{L}_{REE} = \arg \min_{\phi'} \mathbb{E}_q \left[\mathbf{d}(\mathbf{x}, G_\psi(E_{\phi'}(\mathbf{x}))) \right. \\ \left. + \mathbf{d}(G_\psi(E_{\phi'}(\mathbf{x})), G_\psi(E_{\phi'}(\mathbf{x} + \delta))) \right]. \end{aligned} \quad (11)$$

In summary, the self-supervised training process of robust encoder with prior VAE-WGAN is depicted in Fig. 2 and illustrated in Algorithm 1.

D. Out-of-Domain Latent Space

Currently, one of the biggest application bottlenecks of DL-based SemCom is their generalization performance, which means that these machine learning models will significantly degrade their performances when facing data types that are not included in the training dataset (*out-of-domain*). For the proposed VAE-WGAN architecture based SemCom, when the transmitter wants to send an *out-of-domain* data, the robust

Algorithm 1: Training algorithm of robust GAN inversion $E_{\phi'}(\cdot)$

Input: Dataset $q(\mathbf{x})$, learning rate η_1 and η_2 , original encoder $E_\phi(\cdot)$, generator $G_\psi(\cdot)$,
Output: The updated robust encoder $E_{\phi'}(\cdot)$

- 1 **Initialize** $\phi' \leftarrow \phi$;
- 2 **repeat**
- 3 Sample $\mathbf{x} \sim q(\mathbf{x})$;
- 4 Initialize $\delta^0 \leftarrow \mathbf{0}$ and $i \leftarrow 1$;
- 5 **repeat**
- 6 Compute $\delta^i \leftarrow P_C(\delta^{i-1} - \eta_1 \nabla_{\delta} e(\delta^{i-1}))$;
- 7 Update $i \leftarrow i + 1$;
- 8 **until** *Converged*;
- 9 Determine δ by $\delta \leftarrow \delta^k$;
- 10 Update ϕ' by

$$\phi' \leftarrow \phi' - \eta_2 \nabla_{\phi'} \left[\mathbb{E}_q(\mathbf{d}(\mathbf{x}, G_\psi(E_{\phi'}(\mathbf{x}))) + \mathbf{d}(G_\psi(E_{\phi'}(\mathbf{x})), G_\psi(E_{\phi'}(\mathbf{x} + \delta))) \right];$$
- 11 **until** *Converged*;
- 12 **Return** Robust GAN inversion $E_{\phi'}(\cdot)$

encoder $E_{\phi'}$ may encode an abnormal latent vector, and the decoder at the receiver will reconstruct data that is semantically different from the transmitted data. For this reason, when facing the data with unknown distributions, JSCC should improve its generalization abilities and be able to quickly adapt to search for the optimal *out-of-domain* latent space.

To address this issue, a learning-based adaptor constructed by a lightweight single-layer neural network is utilized for *out-of-domain* latent space determination. Considering the characteristics of VAE-WGAN, as shown in Fig. 3, the adaptor $g_\omega(\cdot)$ parameterized by ω is placed between the robust encoder and generator. Subsequently, when the transmitted data follows an unknown distribution, adaptor $g_\omega(\cdot)$ can perform one-shot learning to transform the latent vector \mathbf{z} encoded by $E_{\phi'}(\cdot)$ into

$$\hat{\mathbf{z}} = g_\omega(\mathbf{z}) = \omega^\top \mathbf{z} + \mathbf{b}, \quad (12)$$

where \mathbf{b} denotes the bias of adaptor $g_\omega(\cdot)$. In order to improve the data quality of reconstruction, inspired by the adversarial training strategy of WGAN, this paper considers another adaptor $d_\nu(\cdot)$ composed of a lightweight fully connected (FC) layer for adversarial training with $g_\omega(\cdot)$. As illustrated in Fig. 3, during online training, the FC layer of discriminator $D_\gamma(\cdot)$ is replaced by $d_\nu(\cdot)$, and the original discriminator after removing the FC layer is denoted by $d_\gamma(\cdot)$. In this way, the online training process of $g_\omega(\cdot)$ is similar to WGAN's training approach as illustrated in Algorithm 2.

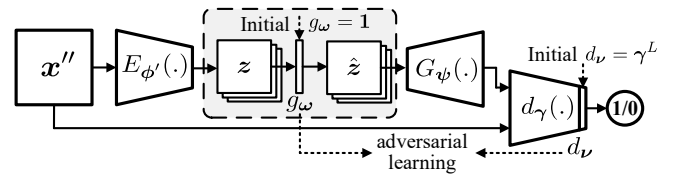


Fig. 3. *Out-of-domain* latent space determination using lightweight single-layer network and adversarial training method.

In summary, when the SemCom system transmits data *in domain*, the parameters ω of $g_\omega(\cdot)$ is equal to $\mathbf{1}$, while transmitting data with significant reconstruction errors, online

Algorithm 2: Online training algorithm of out-of-distribution adaptor $g_\omega(\cdot)$

Input: Data following unknown distribution $q(\mathbf{x}'')$, learning rate η , gradient penalty coefficient λ , robust encoder $E_{\phi'}(\cdot)$, generator $G_\psi(\cdot)$, discriminator $D_\gamma(\cdot)$ and the parameters of last layer (L-th layer) is denoted by γ^L

Output: The online-updated adaptor $g_\omega(\cdot)$

```

1 Initialize  $\omega \leftarrow \mathbf{1}$  and  $\nu \leftarrow \gamma^L$ ;
2 repeat
3   Sample  $\mathbf{x}'' \sim q(\mathbf{x}'')$ ,  $\mathbf{z} \sim q_\psi(\mathbf{z})$ , and  $\epsilon \sim U[0, 1]$ ;
4   Compute  $\hat{\mathbf{x}} \leftarrow \epsilon \mathbf{x}'' + (1 - \epsilon)G_\psi(g_\omega(\mathbf{z}))$ ;
5   Update  $\nu \leftarrow \nu - \eta \nabla_\nu \left[ \mathbb{E}_q(-d_\nu(d_\gamma(\mathbf{x}''))) + \right.$ 
       $\left. d_\nu(d_\gamma(G_\psi(g_\omega(\mathbf{z})))) + \lambda(\|\nabla_{\hat{\mathbf{x}}} d_\nu(d_\gamma(\hat{\mathbf{x}}))\|_2 - 1)^2 \right]$ ;
6   Update  $\omega \leftarrow \omega - \eta \nabla_\omega \left[ \mathbb{E}_q(-d_\nu(d_\gamma(G_\psi(g_\omega(\mathbf{z})))) \right]$ ;
7 until Converged;
8 Return the parameters  $\omega$  of adaptor  $g_\omega(\cdot)$ 

```

learning Algorithm 2 will be activated. Due to the limited amount of training data and the fact that the given initial values of $\hat{\mathbf{z}}$ and ω are close to the optimal values, this online-updated process will be very fast. When the online-learning is completed, in order to not change the weights ϕ' , ψ , and θ of robust encoder, generator, and LDM utilized for channel denoising, the adaptor is deployed at the receiver and defined as a dynamic lightweight neural network. In other words, the parameters of the implemented adaptor $g_\omega(\cdot)$ can be dynamically changed in the proposed SemCom system as shown in Fig. 1. Ultimately, the semantically consistent *out-of-domain* data is reconstructed according to $\hat{\mathbf{z}} = g_\omega(\mathbf{z})$.

IV. LATENT CHANNEL DENOISING DIFFUSION MODEL

In this section, the wireless channel equalization under different conditions is firstly established in Subsection IV-A. The training objectives of original LDMs based on the received signals and its one-step real-time implementation are introduced in Subsections IV-B and IV-C.

A. Wireless Channel Equalization

Given the JSCC composed of robust encoder $E_{\phi'}(\cdot)$ and generator $G_\psi(\cdot)$, the robust encoder encodes the original data \mathbf{x} into a low-dimensional latent bottleneck \mathbf{z} . Assume that the latent vector \mathbf{z} needs to reach the receiver through wireless channel by k times, the transmitted complex latent signal is denoted by $\mathbf{z}_c \in \mathbb{C}^k$. At time t , the i -th symbol of complex signal \mathbf{y}_c received by the receiver can be represented as

$$y_{c,i} = h_{c,i}z_{c,i} + n_{c,i}, \quad (13)$$

where $h_{c,i} = \sum_{p=1}^P \alpha_p e^{-j2\pi f \tau_p(t)}$, α_p is the signal amplitude of the p -th path, P denotes the number of paths, f is the carrier frequency, $\tau_p(t)$ denotes the phase shift, $n_{c,i} \sim \mathcal{CN}(0, \sigma^2)$ represents the complex Gaussian noise. Considering the effects of multipath fading and scattering, $h_{c,i}$ are independent and identically distributed (i.i.d.) Rician fading gains, which can be denoted by

$$h_{c,i} = \sqrt{\frac{K}{K+1}} + \sqrt{\frac{1}{K+1}} h_{Rayleigh,i}, \quad (14)$$

where $h_{Rayleigh,i}$ are i.i.d. Rayleigh fading gains and K is the ratio of direct radio waves' power and non-direct radio waves' power. When $K = \infty$, the wireless channel becomes additive white Gaussian noise (AWGN) channel, and the channel becomes Rayleigh channel when $K = 0$. Optionally, minimum mean square error (MMSE) is utilized as a method for received signals equalization to avoid errors and improve efficiency. Consequently, let $\mathbf{h}_c = [h_{c,1}, \dots, h_{c,k}]$ and $\mathbf{n}_c = [n_{c,1}, \dots, n_{c,k}]$ be the channel state and noises, the addressed signals can be denoted by

$$\begin{aligned} \mathbf{y}_{eq} &= (\mathbf{h}_c^H \mathbf{h}_c + \sigma^2 \mathbf{I})^{-1} \mathbf{h}_c^H (\mathbf{h}_c \mathbf{z}_c + \mathbf{n}_c) \\ &= (\mathbf{h}_c^H \mathbf{h}_c + \sigma^2 \mathbf{I})^{-1} \mathbf{h}_c^H \mathbf{h}_c \mathbf{z}_c + (\mathbf{h}_c^H \mathbf{h}_c + \sigma^2 \mathbf{I})^{-1} \mathbf{h}_c^H \mathbf{n}_c. \end{aligned} \quad (15)$$

For simplicity, the transmitted complex signals \mathbf{z}_c can also be rewritten as $\mathbf{z}_R \in \mathbb{R}^{2k}$ in real-valued symbols, the output of equalization can be also decoupled as corresponding real-valued $\mathbf{y}_R \in \mathbb{R}^{2k}$. In this way, the 1-st to k -th signals of \mathbf{y}_R are

$$y_{R,i} = \frac{|h_{c,i}|^2}{|h_{c,i}|^2 + \sigma^2} z_{R,i} + \frac{Re(h_{c,i}^H)}{|h_{c,i}|^2 + \sigma^2} \sigma \epsilon, \quad (16)$$

where $\epsilon \sim \mathcal{N}(0, 1)$. And the $k+1$ -th to $2k$ -th signals can be defined as

$$y_{R,i} = \frac{|h_{c,i}|^2}{|h_{c,i}|^2 + \sigma^2} z_{R,i} + \frac{Im(h_{c,i}^H)}{|h_{c,i}|^2 + \sigma^2} \sigma \epsilon. \quad (17)$$

To this end, the known diagonal channel state matrix \mathbf{H}_z and noise coefficient matrix \mathbf{H}_n can be defined as

$$\mathbf{H}_z = \text{diag} \left(\frac{|h_{c,1}|^2}{|h_{c,1}|^2 + \sigma^2}, \dots, \frac{|h_{c,k}|^2}{|h_{c,k}|^2 + \sigma^2}, \frac{|h_{c,1}|^2}{|h_{c,1}|^2 + \sigma^2}, \dots, \frac{|h_{c,k}|^2}{|h_{c,k}|^2 + \sigma^2} \right), \quad (18)$$

$$\mathbf{H}_n = \text{diag} \left(\frac{Re(h_{c,1}^H)}{|h_{c,1}|^2 + \sigma^2}, \dots, \frac{Re(h_{c,k}^H)}{|h_{c,k}|^2 + \sigma^2}, \frac{Im(h_{c,1}^H)}{|h_{c,1}|^2 + \sigma^2}, \dots, \frac{Im(h_{c,k}^H)}{|h_{c,k}|^2 + \sigma^2} \right). \quad (19)$$

As a consequence, the conditional distribution of \mathbf{y}_R under the estimated wireless CSI, i.e., \mathbf{h}_c and SNRs, is

$$q_{\text{MMSE}}(\mathbf{y}_R | \mathbf{z}_R, \mathbf{H}_z, \mathbf{H}_n) = \mathcal{N}(\mathbf{y}_R; \mathbf{H}_z \mathbf{z}_R, \mathbf{H}_n \sigma^2 \mathbf{I}), \quad (20)$$

which means the received signals is affected by the channel's fading gains and noises. Especially, $\mathbf{H}_z = \mathbf{H}_n = \mathbf{I} \in \mathbb{R}^{2k \times 2k}$ under AWGN channel.

B. Latent Diffusion Model

The denoising task of receiver is to find the original transmitted signals \mathbf{z}_R from transmitter given \mathbf{y}_R and CSI. Accordingly, let $\mathbf{z}_0 = \mathbf{H}_z \mathbf{z}_R$, the cross-entropy term in SemCom system model can be transformed from $\mathbb{E}_{q_\phi(\mathbf{z}|\mathbf{x})}[-\log p_\theta(\mathbf{z})]$ to $\mathbb{E}_q[-\log p_\theta(\mathbf{z}_0 | \mathbf{y}_R, \mathbf{H}_z, \mathbf{H}_n)]$. LDM is selected for wireless channel denoising as it has powerful capabilities to generate realistic data and much lower computational complexity than the original DMs. Let $\{\mathbf{z}_t\}_{t=0}^{T-1}$ be the noisy latent bottlenecks containing noises of different SNRs in the continuous time

domain $t \in [0, T]$, where \mathbf{z}_0 is the starting latent vector. LDM defines a forward process through a unified stochastic differential equation (SDE)

$$d\mathbf{z} = \mathbf{u}(\mathbf{z}, t)dt + \mathbf{g}(t)d\mathbf{w}_t, \quad (21)$$

where $\mathbf{u}(\mathbf{z}, t)$ and $\mathbf{g}(t)$ are the drift and diffusion coefficients, and \mathbf{w}_t is a standard Brownian motion. By considering the reverse process of SDE, the marginal distribution $p(\mathbf{z}_t)$ follows the solution trajectory of the probability flow-ODE (PF-ODE)

$$d\mathbf{z} = \left[\mathbf{u}(\mathbf{z}, t) - \frac{1}{2}\mathbf{g}^2(t)\nabla_{\mathbf{z}} \log p(\mathbf{z}_t) \right] dt, \quad (22)$$

where $\nabla_{\mathbf{z}} \log p(\mathbf{z}_t)$ denotes the score function. Accordingly, similar to Elucidated DM (EDM) [54], considering the conditional distribution in Eq. (20), this paper sets $\mathbf{u}(\mathbf{z}, t) = 0$, $\mathbf{g}(t) = \sqrt{2t}\mathbf{H}_n$, and $\sigma(t) = \mathbf{H}_n t$, where $t \in [0, T]$. When solving the reverse sampling trajectory, t requires a discrete schedule $\{t_n\}_{n=0}^{n=N}$. Concretely, when $n = 0$, $t_0 = 0$, and when $n \geq 1$, $t_n = \left(t_1^{1/\rho} + \frac{n-1}{N-1} \left(t_N^{1/\rho} - t_1^{1/\rho} \right) \right)^\rho$, where $\rho > 0$. Moreover, unlike denoising diffusion probabilistic model (DDPM) [23], the utilized diffusion model adopts variance explosion (VE) strategy, and its associated forward process $\{\mathbf{z}_t\}_{t=0}^{t=T}$ can be written as

$$q(\mathbf{z}_t|\mathbf{z}_0) = \mathcal{N}(\mathbf{z}_t; \mathbf{z}_0, t^2 \mathbf{H}_n^2 \mathbf{I}). \quad (23)$$

In the reverse process, the denoising U-Net is usually utilized to predict approximation function $\mathbf{s}_\theta(\mathbf{z}, t)$ to approximate the score function $\nabla_{\mathbf{z}} \log p(\mathbf{z}_t)$. Noise prediction model $\epsilon_\theta(\mathbf{z}_t, t)$ is one of the most popular implementations of diffusion models, and $\mathbf{s}_\theta(\mathbf{z}, t) = -\frac{\epsilon_\theta(\mathbf{z}_t, t)}{\mathbf{H}_n t}$ [55]. As a consequence, the training objective of LDM is to minimize the distance between noise prediction $\epsilon_\theta(\mathbf{z}_t, t)$ and actual noise ϵ [55]

$$\begin{aligned} \mathcal{L}_{LDM} &= \mathbb{E}_q \left[\left\| \mathbf{s}_\theta(\mathbf{z}, t) - \nabla_{\mathbf{z}} \log p(\mathbf{z}_t) \right\|_2^2 \right] \\ &= \mathbb{E}_{\mathbf{z}_R, \epsilon_1, n} \left[\left\| \frac{\epsilon_\theta(\mathbf{H}_z \mathbf{z}_R + \mathbf{H}_n t_n \epsilon_1, t_n)}{\mathbf{H}_n t_n} - \frac{\epsilon}{\mathbf{H}_n t_n} \right\|_2^2 \right] \\ &\Leftrightarrow \mathbb{E}_q \left[\left\| \epsilon_\theta(\mathbf{z}_t, t) - \epsilon \right\|_2^2 \right], \end{aligned} \quad (24)$$

where $\epsilon_1 \sim \mathcal{N}(\mathbf{0}, \mathbf{I})$ and $n \sim \mathcal{U}[1, N]$. Considering aforementioned conditions and settings, the PF-ODE defined in Eq. (22) can be rewritten as

$$\frac{d\mathbf{z}_t}{dt} = \epsilon_\theta(\mathbf{z}_t, t). \quad (25)$$

Similar to the channel denoising DM in [37], wireless channel denoising task is a subprocess of whole diffusion reverse process. The denoising start point t_m should be determined by $\arg \min_{t_m} |\sigma^2 - t_m^2|$ with known σ^2 and m denotes the utilized denoising steps of pretrained LDM. Consequently, The selection of hyperparameters N and T should consider the worst-case SNRs to make the channel denoising objective a sub-term of the DM training objective. Ultimately, the transmitted latent vector \mathbf{z}_R is given by $\mathbf{H}_z^{-1} \mathbf{z}_0$. Nonetheless, in the wireless communication scenarios with large noise variance σ^2 , $m \gg 1$ according to the designed discrete schedule $\{t_n\}_{n=0}^{n=N}$. As a result, LDM will execute m times of noise

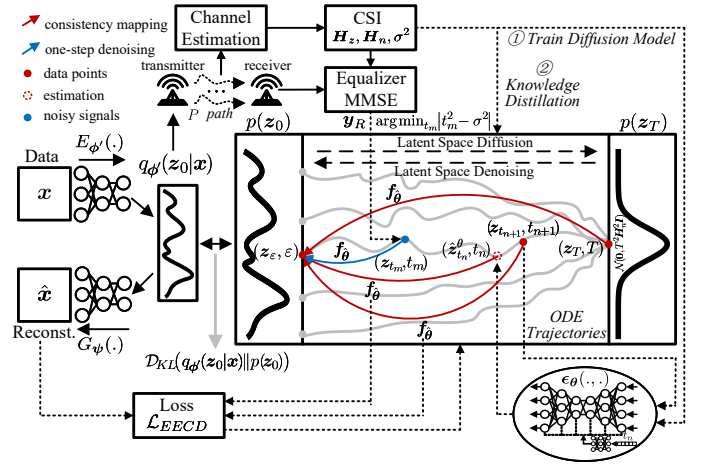


Fig. 4. In the proposed SemCom model, data is mapped into latent space via robust encoder $q_{\psi'}(\mathbf{z}_0|\mathbf{x})$. Then, EECD maps noisy received signals to denoised latent vector ($\mathbf{z}_{t_m} \rightarrow \mathbf{z}_{\epsilon}$) and decoder will generate data with desired semantic meaning by $p_{\psi}(\mathbf{x}|\mathbf{z}_{\epsilon})$.

predictions $\epsilon_\theta(\mathbf{z}_t, t)$, i.e., the number of function evaluations (NFE) will reach m . Unfortunately, the varying fading wireless channels with uncertain SNRs bring significant uncertainties to the computational complexity of LDM, which undermines the possibility of implementing real-time SemCom.

C. End-to-End Consistency Distillation

The multi-step reverse sampling process of DMs brings the disadvantage of slow data generation speed. To overcome it, methods based on DDIM subsequence sampling [24], optimal reverse variances [56], LDMs [45], SDE/ODE solvers [55], [57], and knowledge distillation [43], [58] have been proposed to optimize or accelerate the sampling process. In detail, the LDMs can significantly reduce the dimensionality of input data, and some distillation based approaches only require a few steps or even one step to evaluate the output data without generation quality issues. Among these acceleration methods, the consistency model [43], as one of the distillation approaches, defines the consistency function $\mathbf{f} : (\mathbf{z}_t, t) \mapsto \mathbf{z}_\epsilon$ given a forward trajectory $\{\mathbf{z}_t\}_{t \in [\epsilon, T]}$, where $\epsilon = t_1 \approx 0$. The consistency function assumes that for the input data on the same forward trajectory, the output of the neural network parameterized function points to the same generated data, which is given by

$$\mathbf{f}_{\hat{\theta}}(\mathbf{z}_t, t) = \begin{cases} \mathbf{z}_t & t = \epsilon \\ \mathbf{F}_{\hat{\theta}}(\mathbf{z}_t, t) & t \in (\epsilon, T], \end{cases} \quad (26)$$

where $\hat{\theta}$ is the neural network parameters of consistency model. By observing function $\mathbf{F}_{\hat{\theta}}(\mathbf{z}_t, t)$, it can be implemented by directly training a neural network to map noisy data $\{\mathbf{z}_t\}_{t \in (\epsilon, T]}$ to \mathbf{z}_ϵ . Accordingly, the consistency function $\mathbf{f}_{\hat{\theta}}(\mathbf{z}_t, t)$ can be obtained based on EDM architecture by distilling the pretrained original LDM $\epsilon_\theta(\mathbf{z}_t, t)$.

Assume that the time schedule of the sampling process is $\epsilon = t_1 < T_2 < \dots < t_N = T$, the Euler solver is adopted for reverse process evaluation. As a result, at $t = t_{n+1}$, Eq. (25)

Algorithm 3: Training algorithm of EECD

Input: Dataset $q(\mathbf{x})$, initial model parameter $\hat{\theta}$, robust encoder $E_\phi(\cdot)$, generator $G_\psi(\cdot)$, pretrained latent diffusion model $\epsilon_\theta(\cdot, \cdot)$, distance metric $\mathbf{d}(\cdot, \cdot)$, learning rate η , decay rate μ , time schedule $\{t_n\}_{t=1}^{t=N}$, and channel state information $\mathbf{H}_z, \mathbf{H}_n$

Output: The trained one-step end-to-end consistency model

```

1 Initialize  $\hat{\theta}^- \leftarrow \hat{\theta}$ ;
2 repeat
3   Sample  $\mathbf{x} \sim q(\mathbf{x})$  and  $n \sim \mathcal{U}[1, N-1]$ ;
4   Compute  $\mathbf{z} \leftarrow E_\phi(\mathbf{x})$  and transmitted  $\mathbf{z}_R$ ;
5   Sample  $\mathbf{z}_{t_{n+1}} \sim \mathcal{N}(\mathbf{z}_{t_{n+1}}; \mathbf{H}_z \mathbf{z}_R, t_{n+1}^2 \mathbf{H}_n^2 \mathbf{I})$ ;
6   Compute  $\tilde{\mathbf{z}}_{t_n}^\theta \leftarrow \mathbf{z}_{t_{n+1}} - \epsilon_\theta(\mathbf{z}_{t_{n+1}}, t_{n+1})(t_{n+1} - t_n)$ ;
7   Estimate  $\mathbf{z}_{t_n}$  by  $\tilde{\mathbf{z}}_{t_n}^\theta \leftarrow$ 
    $\mathbf{z}_{t_{n+1}} - \frac{1}{2} [\epsilon_\theta(\tilde{\mathbf{z}}_{t_n}^\theta, t_n) + \epsilon_\theta(\mathbf{z}_{t_{n+1}}, t_{n+1})](t_{n+1} - t_n)$ ;
8   Compute  $\mathcal{L}_{EECD}(\hat{\theta}, \hat{\theta}^- | \theta, \psi)$  by Eq. (31);
9   Update  $\hat{\theta} \leftarrow \hat{\theta} - \eta \nabla_{\hat{\theta}} \mathcal{L}_{EECD}(\hat{\theta}, \hat{\theta}^- | \theta, \psi)$ ;
10  Update  $\hat{\theta}^- \leftarrow \text{stopgrad}(\mu \hat{\theta}^- + (1 - \mu) \hat{\theta})$ ;
11 until Converged;
12 Return End-to-end distilled consistency model  $\mathbf{f}_{\hat{\theta}}(\cdot, \cdot)$ 

```

can be transformed into

$$\begin{aligned} \frac{d\mathbf{z}_t}{dt} \Big|_{t=t_{n+1}} &= \epsilon_\theta(\mathbf{z}_{t_{n+1}}, t_{n+1}) \approx \frac{\mathbf{z}_{t_{n+1}} - \mathbf{z}_{t_n}}{t_{n+1} - t_n} \\ \Leftrightarrow \tilde{\mathbf{z}}_{t_n}^\theta &\approx \mathbf{z}_{t_{n+1}} - \epsilon_\theta(\mathbf{z}_{t_{n+1}}, t_{n+1})(t_{n+1} - t_n), \end{aligned} \quad (27)$$

where $\tilde{\mathbf{z}}_{t_n}^\theta$ denotes the predicted data point at $t = t_n$. This is also called denoising diffusion implicit model (DDIM) [24] and every step's NFE equals to 1. However, the actual values of the difference $\frac{\mathbf{z}_{t_{n+1}} - \mathbf{z}_{t_n}}{t_{n+1} - t_n}$ are closer to the derivatives between $\mathbf{z}_{t_{n+1}}$ and \mathbf{z}_{t_n} , rather than the derivative at $\mathbf{z}_{t_{n+1}}$. To this end, the Heun solver in EDM is adopted [54], which is denoted by

$$\begin{aligned} \frac{\mathbf{z}_{t_{n+1}} - \mathbf{z}_{t_n}}{t_{n+1} - t_n} &\approx \frac{1}{2} (\epsilon_\theta(\mathbf{z}_{t_n}, t_n) + \epsilon_\theta(\mathbf{z}_{t_{n+1}}, t_{n+1})) \Leftrightarrow \\ \tilde{\mathbf{z}}_{t_n}^\theta &\approx \mathbf{z}_{t_{n+1}} - \frac{1}{2} (\epsilon_\theta(\mathbf{z}_{t_n}, t_n) + \epsilon_\theta(\mathbf{z}_{t_{n+1}}, t_{n+1})) (t_{n+1} - t_n), \end{aligned} \quad (28)$$

where \mathbf{z}_{t_n} on the right side of Eq. (28) can be approximated by $\tilde{\mathbf{z}}_{t_n}^\theta$ in Eq. (27). Consequently, the estimation of \mathbf{z}_{t_n} is given by

$$\tilde{\mathbf{z}}_{t_n}^\theta \approx \mathbf{z}_{t_{n+1}} - \frac{1}{2} (\epsilon_\theta(\tilde{\mathbf{z}}_{t_n}^\theta, t_n) + \epsilon_\theta(\mathbf{z}_{t_{n+1}}, t_{n+1})) (t_{n+1} - t_n), \quad (29)$$

where the NFE equals to 2. According to the definition of the consistency function, the function $\mathbf{f}_{\hat{\theta}}(\mathbf{z}_t, t)$ should have the same output for adjacent data points $(\mathbf{z}_{t_{n+1}}, t_{n+1})$ and $(\tilde{\mathbf{z}}_{t_n}^\theta, t_n)$ on the same reverse trajectory, i.e., the loss of the consistency model is

$$\mathcal{L}_{CD}(\hat{\theta}, \hat{\theta}^- | \theta) = \mathbb{E}_q [\mathbf{d}(\mathbf{f}_{\hat{\theta}}(\mathbf{z}_{t_{n+1}}, t_{n+1}), \mathbf{f}_{\hat{\theta}^-}(\tilde{\mathbf{z}}_{t_n}^\theta, t_n))], \quad (30)$$

where $\hat{\theta}^-$ denotes the running average of the past values of $\hat{\theta}$ during optimization. Nonetheless, the goal of wireless SemCom is to accurately reconstruct the transmitted data in real-time manner in the receiver side. Inspired by that, the consistency distillation (CD) loss in Eq. (30) can be changed

to the loss of EECD, which is given by

$$\begin{aligned} \mathcal{L}_{EECD}(\hat{\theta}, \hat{\theta}^- | \theta, \psi) \\ = \mathbb{E}_q [\mathbf{d}(G_\psi(\mathbf{f}_{\hat{\theta}}(\mathbf{z}_{t_{n+1}}, t_{n+1})), G_\psi(\mathbf{f}_{\hat{\theta}^-}(\tilde{\mathbf{z}}_{t_n}^\theta, t_n)))], \end{aligned} \quad (31)$$

where $\mathbf{d}(\cdot, \cdot)$ is denoted by Euclidean distance for non-images datasets, and structural similarity index measure (SSIM) or learned perceptual image path similarity (LPIPS) [59] based distance for image datasets.

The distillation training process of EECD is illustrated in Algorithm 3. As depicted in Fig. 4, the student model $\mathbf{f}_{\hat{\theta}}(\cdot, \cdot)$ updates its parameters $\hat{\theta}$ and $\hat{\theta}^-$ through gradient descent by minimizing the perceptual loss \mathcal{L}_{EECD} between the decoded data $(\mathbf{x}_{t_{n+1}}, t_{n+1})$ and $(\hat{\mathbf{x}}_{t_n}^\theta, t_n)$ corresponding to the original latent space data point $(\mathbf{z}_{t_{n+1}}, t_{n+1})$ and the next point $(\tilde{\mathbf{z}}_{t_n}^\theta, t_n)$ in the reverse diffusion process predicted by the diffusion (teacher) model. This process ensures the consistency of direct mapping to \mathbf{z}_ε along the same ODE trajectory. Additionally, in the sampling phase, the pretrained latent consistency model can flexibly enhance the perceptual quality of reconstruction by resampling $s - 1$ times based on the subsequence $\tau = [\tau_1, \tau_2, \dots, \tau_s]$ of length s , where $\tau_1 = m$. Consequently, the real-time channel denoising and data reconstruction process based on EECD model is given in Algorithm 4. The advantages of utilizing the enhanced loss term to distill LDM are further elaborated as follows:

- The training of the original LDM cannot optimize the generation of latent space together with the decoder $G_\psi(\cdot)$. However, the proposed end-to-end consistency loss allows the training objective to no longer be limited to mapping received noisy signal \mathbf{y}_R after equalization to the denoised latent space $\hat{\mathbf{z}}_0$, but directly measures the distance of adjacent data points on the same trajectory.
- The latent consistency model cannot directly utilize more superior semantic metrics such as LPIPS to enhance perceptual quality, while the EECD based loss effectively eliminates the limitation of only being able to calculate the Euclidean distance between two latent bottlenecks.

V. NUMERICAL EXPERIMENTS

A. Experimental Setup

1) *Dataset:* MNIST handwritten digit image dataset is initially considered for evaluating the proposed SemCom system, containing 60,000 images for training and 10,000 for testing. Additionally, to validate the performance of *out-of-domain* adaptation, the Fashion-MNIST (F-MNIST) dataset is also employed in the evaluation, comprising images of various types of clothing and accessories, with an identical distribution of 60,000 training and 10,000 testing images. The resolution for both MNIST and F-MNIST datasets are uniformly resized to 32×32 . Furthermore, the animal face high quality (AFHQ) dataset [60] is also selected to verify the effectiveness of the proposed method, including a total of 15,000 RGB images across three categories: dogs, cats, and wild animals, where 4,500 images of dogs are used for training and the remaining 500 dog images, along with 500 cat images, are used to test the proposed method, with the resolution resized to 192×192 .

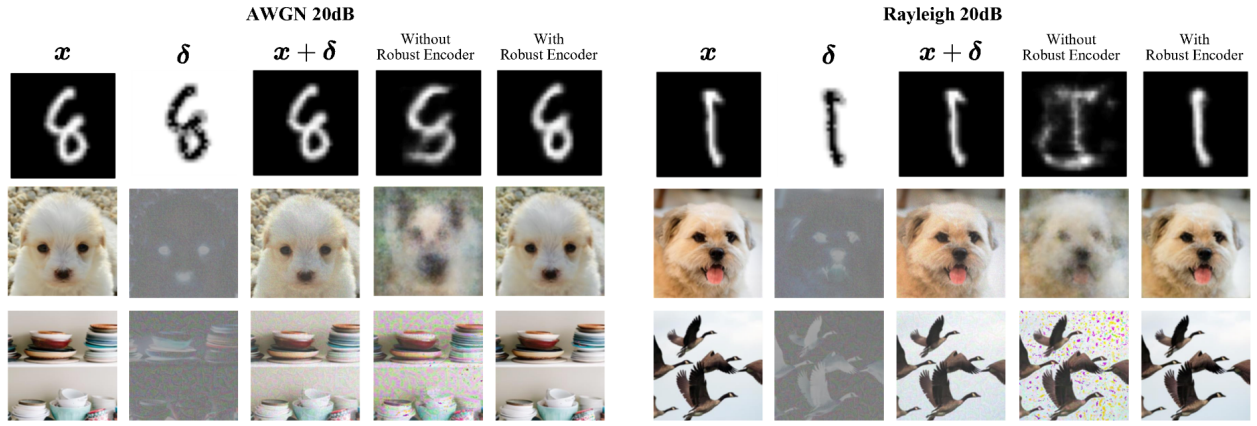


Fig. 5. Some typical decoded images without/with robust encoder under AWGN and Rayleigh channel. The SNR is 20dB.

Algorithm 4: Sampling of channel denoising EECD

Input: Transmitted data \mathbf{x} , robust encoder $E_{\phi'}(\cdot)$, generator $G_{\psi}(\cdot)$, distilled end-to-end consistency model $\mathbf{f}_{\hat{\theta}}(\cdot, \cdot)$, subsequence length s , and channel state information $\mathbf{H}_z, \mathbf{H}_n, \sigma$

Output: Reconstructed data $\hat{\mathbf{x}}$ at the receiver

- 1 Compute the encoded latent space $\mathbf{z} \leftarrow E_{\phi'}(\mathbf{x})$;
 - 2 Transmit real-valued \mathbf{z}_R through noisy wireless channel;
 - 3 Compute MMSE equalization $\mathbf{y}_R \leftarrow \mathbf{H}_z \mathbf{z}_R + \mathbf{H}_n \sigma \epsilon$ and $\epsilon \sim \mathcal{N}(\mathbf{0}, \mathbf{I})$;
 - 4 Estimate t_m by $\arg \min_{t_m} |t_m^2 - \sigma^2|$;
 - 5 Compute denoised estimation $\hat{\mathbf{z}}_{\epsilon} \leftarrow \mathbf{f}_{\hat{\theta}}(\mathbf{y}_R, t_m)$;
 - 6 **if** $s > 1$ **then**
 - 7 Determine subsequence $\tau = [\tau_1, \tau_2, \dots, \tau_s]$;
 - 8 **for** $i = 2$ **to** s **do**
 - 9 Sample $\mathbf{z}_{t_{\tau_i}} \sim \mathcal{N}(\mathbf{z}_{t_{\tau_i}}; \hat{\mathbf{z}}_{\epsilon}, t_{\tau_i}^2 \mathbf{H}_n^2 \mathbf{I})$;
 - 10 Compute $\hat{\mathbf{z}}_{\epsilon} \leftarrow \mathbf{f}_{\hat{\theta}}(\mathbf{z}_{t_{\tau_i}}, t_{\tau_i})$;
 - 11 **end**
 - 12 **end**
 - 13 Compute denoised data $\hat{\mathbf{z}}_R \leftarrow \mathbf{H}_z^{-1} \hat{\mathbf{z}}_{\epsilon}$ and decoded $\hat{\mathbf{z}}$;
 - 14 **Return** the recovered data $\hat{\mathbf{x}} \leftarrow G_{\psi}(\hat{\mathbf{z}})$
-

Lastly, the DIV2K high-quality RGB image dataset [61] is also considered for SemCom tasks, encompassing 800 diverse training images, 100 validation images, and 100 test images, with the resolution resized to 256×256.

2) *Baseline Method:* Three distinct implementations of communication systems are utilized for comparison to demonstrate the superiority of the proposed SemCom system. The first is a combination of the state-of-the-art traditional image compression method JPEG2000 [10] with the error correction technique low-density parity check (LDPC) [62], denoted as JPEG2000+LDPC. The second is the widely recognized VAE-based JSCC method [6], where joint source-channel training effectively mitigates the adverse effects of unreliable channels. The final approach is the multi-step VE-based LDM (VE-LDM) [37], which also serves as the teacher model for subsequent knowledge distillation.

3) *Performance Metrics:* The metrics for model evaluation can broadly be categorized into two types. The first category encompasses traditional image reconstruction metrics for bit/symbol accuracy, including measures such as mean squared error (MSE)↓ and peak SNR (PSNR)↑, where ↑ indicates that a higher value represents better performance, while ↓ indicates the opposite. The second category consists of semantic

or human-perceptual metrics that warrant increased attention within the context of SemCom. For image transmission, this includes the SSIM and multi-scale SSIM (MS-SSIM)↑ [15] and the pretrained VGG-based LPIPS↓ [59].

4) *CSI Condition:* For the wireless channels, three distinct channels are taken into consideration, including the AWGN channel ($K = \infty$), the Rayleigh channel ($K = 0$), and the Rician channel ($K = 1$). Regarding the noise level of the channels, noise with SNRs ranging from 0dB to 20dB is contemplated for testing the performance of various methods under different SNR conditions. The channel bandwidth ratio (CBR) is defined as $\text{CBR} = k/(H \times W \times C)$, where H , W , and C are the height, width (resolution) and colour channel of images, and usually $H=W$. CBR is also an exceedingly crucial metric in SemCom, defining the demand for communication resources. For this reason, CBRs from 0.01 to 0.05 are implemented on DL models trained by AFHQ and DIV2K datasets, while for the MNIST dataset, due to its low resolution, only the DL with 1/16 CBR and the JPEG2000+LDPC with 1/3 CBR have been realized.

5) *Simulation Environment and Hyperparameters:* The simulations are conducted using Python 3.8.19 and CUDA-accelerated PyTorch 2.3.0 on a computer equipped with an i5-13600KF CPU operating at 3.50GHz, 32 GB of RAM, and an NVIDIA GeForce RTX 4070 GPU. The training for the wireless channel denoising task can follow a shorter time schedule. Consequently, the total length of the forward process for the LDM is set to $N = 100$, with the variance starting point at $t_1 = \epsilon = 0.002$ and the endpoint at $t_N = T = 2$, and $\rho = 7.0$. Furthermore, the learning rate during training is established at 1e-4, with an initial decay rate of 0.95 and a decay rate of 0.99993 for the student model.

B. Robustness to Data Inaccuracies

As stated in Section III-C, the encoder parameters can be updated via augmented learning based on the obtained semantic errors δ . For the MNIST, AFHQ, and DIV2K datasets, pretrained encoders are updated with a learning process at an error level of $\|\delta\|_p / H = 0.3$. Following the update, several prototypical image datasets are employed to test the robust encoder's efficacy in effectively countering data inaccuracies. Fig. 5 illustrates the impact of semantic errors with levels of

0.5 and 0.4 superimposed on the original data under AWGN channel and Rayleigh channel at SNR of 20dB, respectively. It is readily observed that with the proposed robust encoder, the source data with added semantic errors still bear minimal semantic differences from the original data to the human visual perception. However, when the original SemCom system, without a robust encoder, transmits this contaminated data, the decoded output can result in significant semantic errors, as shown in Fig. 5 for the example images in MNIST and AFHQ datasets, and might also lead to extensive artifacts in reconstructed images as seen for the DIV2K dataset. Fortunately, the introduction of the robust encoder successfully overcomes semantic ambiguities that may arise from the contaminated data due to cyber attacks or other types of outliers, ensuring that the decoded data at the receiver still carries the correct semantic information.

To maintain generality, the results of multiple performance tests for various outlier types and levels across different datasets are documented in Table I. Specifically, the CBR is fixed at approximately 0.02 and the test CSI conditions vary in accordance with Section V-A. It is not difficult to observe that the robust encoder, despite only being updated at a semantic error level of 0.3, still maintains robustness compared to the original encoder under other semantic error levels and low-SNR noise contamination, thereby enhancing the quality of decoded data when source data is subject to semantic errors or noises. Furthermore, evaluation metrics such as PSNR/SSIM/MS-SSIM can be improved by several times or even an order of magnitude, while MSE/LPIPS can be reduced by several times or even by an order of magnitude.

C. Out-of-Domain Adaptation

As described in Section III-D, the proposed SemCom system employs a lightweight, single-layer adapter at the transmitter for rapid one-shot learning and transforms the latent space at the receiver, thereby enabling the DL-based SemCom system to adapt to *out-of-domain* data or enhance decoding quality. Specifically, subsets of clothing images from the F-MNIST dataset and cat images from the AFHQ dataset were utilized to validate the efficacy of the adapter. As illustrated in Fig. 6, without the adapter enabled, a SemCom system pretrained with a particular type of data would decode data at the receiver that more closely resembles that specific type of semantic information, leading to severe semantic ambiguity. However, the adapter situated before the generator can swiftly overcome this shortcoming, producing data that is essentially consistent with the original semantics of the transmitted data. Additionally, the original training DL model underperformed on certain test data from the DIV2K dataset, with decoded data exhibiting partial errors. The adapter also enhances communication quality in such instances, eliminating artifacts in the images.

The evolution of performance metrics during the one-shot learning process for the three datasets is depicted in Fig. 7. Evidently, after approximately only 20 epochs, the metrics of decoded data with adapters can be swiftly ameliorated to ideal values, thereby diminishing semantic ambiguities. To

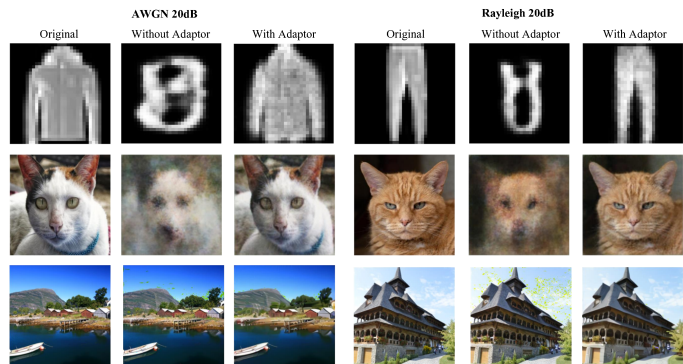


Fig. 6. Some typical decoded images without/with adaptor in AWGN and Rayleigh channel. The SNR is 20dB.

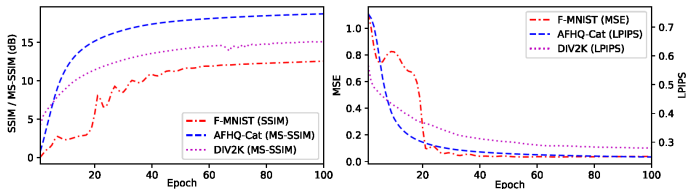


Fig. 7. The performance metrics' curves when doing one-shot learning.

ensure generality, numerical experiments are also conducted to corroborate the effectiveness of the proposed adaptive strategy in enhancing SemCom performance and mitigating semantic ambiguity, with the results presented in Table II. Notably, as evidenced by the semantic evaluation metrics SSIM/MS-SSIM and LPIPS, the incorporation of adapters substantially augments the receiver's *out-of-domain* adaptation and reconstruction capabilities under certain constraints on image categories, preventing the emergence of semantic ambiguities.

D. Channel Denoising Performance

The presence of varying fading gains H_z and noise with uncertain SNRs $H_n\sigma\epsilon$ in wireless channels can severely impair the efficacy of SemCom systems. Accordingly, denoising the noisy signals subsequent to equalization at the receiver emerges as a vital approach to safeguard the desired meaning of the transmitted data. Typically, the channel denoising results of Deep JSCC, JPEG2000+LDPC, VE-LDM, and the proposed EECD methods are demonstrated in Fig. 8 under the conditions of both AWGN and Rayleigh channel at SNR of 10dB. Herein, the conventional JPEG2000+LDPC approach configures CBR at 1/3 for MNIST and 0.05 for AFHQ/DIV2K datasets for higher performances, whereas the CBR for DL-based methods is set at 1/16 for MNIST, and approximately 0.02 for AFHQ/DIV2K. It is noted that JPEG2000+LDPC suffers from partial bit errors and image blurring at a noise level of 10dB SNR, resulting in a lower MS-SSIM and a higher LPIPS than DL-based methods.

Advancing further into DL-based methods, SemCom systems constructed on DMs and GANs outperform those based on a VAE-based Deep JSCC approach. As depicted in Fig. 8, the Deep JSCC method exhibits a slight deficiency in certain image details relative to the latter two methods, leading to marginally inferior semantic metrics. Most crucially, the EECD method, with a subsequence length of $s=2$ used for comparison, demonstrates that the EECD methodology based on VE-LDM distillation virtually matches the performance of

TABLE I
ROBUSTNESS OF SEMANTIC COMMUNICATION SYSTEM UNDER DIFFERENT LEVELS OF SEMANTIC ERRORS AND GAUSSIAN NISOES (WITHOUT ROBUST ENCODER/WITH ROBUST ENCODER), WHERE CBR IS FIXED AT 0.0208 AND CSI IS VARYING

Error/Noise Metric		$\ \delta\ _p / H$					SNR (dB)			
Error/Noise Level		0.1	0.2	0.3	0.4	0.5	5	7.5	10	12.5
MNIST	PSNR (dB)↑	16.54/18.50	11.88/18.52	8.33/18.60	5.96/16.36	5.16/12.42	6.17/8.16	7.52/11.35	10.05/14.91	12.30/17.10
	SSIM (dB)↑	10.65/13.32	5.72/13.56	2.77/13.19	1.18/10.56	0.76/6.79	1.40/3.52	2.21/5.15	4.01/8.60	5.77/11.18
	MSE↓	0.022/0.014	0.065/0.014	0.147/0.013	0.253/0.023	0.304/0.057	0.241/0.153	0.177/0.073	0.099/0.032	0.059/0.019
AFHQ	PSNR (dB)↑	22.31/22.51	18.94/22.14	15.34/21.58	12.82/21.38	9.72/20.58	13.56/15.24	18.45/19.19	21.20/21.89	22.32/21.19
	MS-SSIM (dB)↑	19.82/20.68	13.75/20.65	9.34/20.28	6.56/19.11	3.81/17.76	6.76/9.86	13.42/14.27	17.92/18.44	20.27/20.40
	LPIPS↓	0.160/0.152	0.211/0.157	0.302/0.158	0.410/0.172	0.531/0.180	0.475/0.348	0.246/0.226	0.175/0.172	0.154/0.151
DIV2K	PSNR (dB)↑	23.60/23.71	18.62/23.17	14.55/22.70	10.37/22.01	8.99/21.65	11.87/14.27	16.54/18.66	20.87/21.24	22.20/22.41
	MS-SSIM (dB)↑	16.19/16.49	10.20/16.28	8.22/16.01	6.01/15.88	4.94/15.19	5.66/8.39	11.09/12.73	13.68/15.11	15.35/16.22
	LPIPS↓	0.122/0.121	0.208/0.129	0.325/0.133	0.442/0.147	0.560/0.157	0.512/0.297	0.261/0.237	0.184/0.160	0.131/0.128

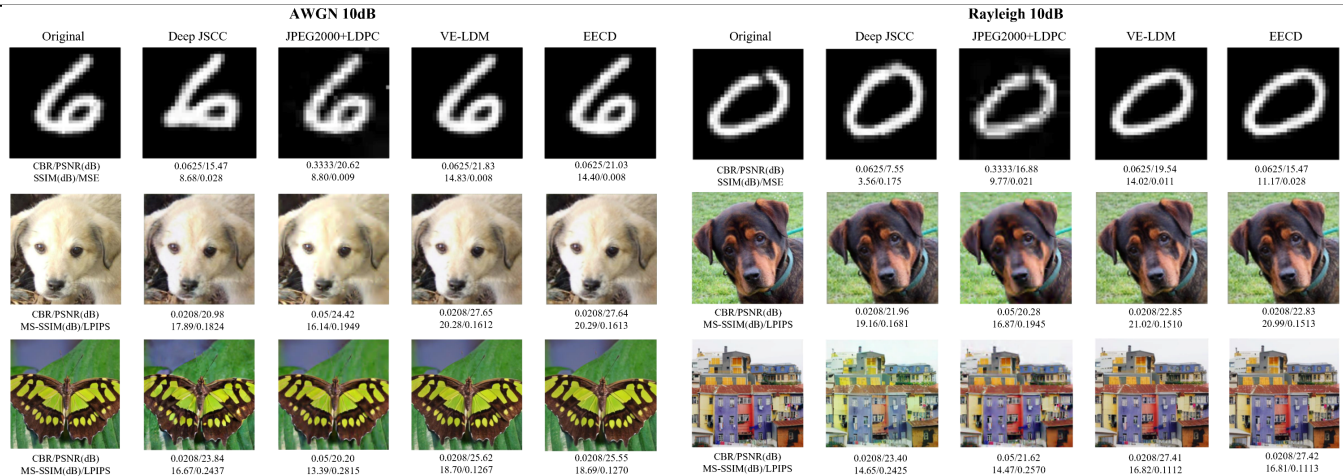


Fig. 8. Some typical decoded images with received signals denoised by different approaches under AWGN and Rayleigh channel. The SNR is 10dB.

TABLE II
IMPROVEMENT IN ADAPATION AND RECONSTRUCTION PERFORMANCE FOR DIFFERENT TYPES OF DATA (WITHOUT ADAPTOR/WITH ADAPTOR)

Dataset	Metrics	PSNR (dB)↑	SSIM/MS-SSIM (dB)↑	MSE/LPIPS↓
F-MNIST		6.16/13.82	0.48/8.90	0.313/0.049
AFHQ-Cat		9.93/19.56	3.09/16.59	0.655/0.232
DIV2K		17.63/28.67	10.51/16.30	0.288/0.175

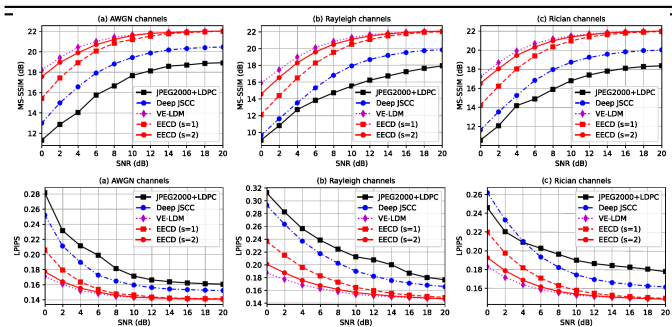


Fig. 9. Semantic metrics of JPEG2000+LDPC, Deep JSCC, VE-LDM, and EECD methods under different SNRs and channel states within AFHQ dataset. the original teacher model at SNR of 10dB, unequivocally attesting to the effectiveness and superiority of the proposed end-to-end human perception metric-based distillation strategy.

Numerical experiments conducted on the AFHQ dataset have provided ample validation for the four distinct methodologies, revealing variations in two pivotal semantic metrics

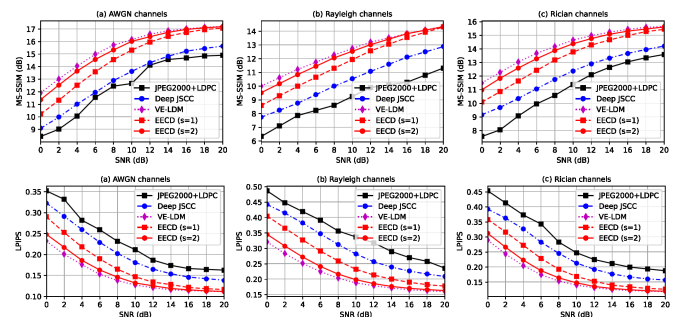


Fig. 10. Semantic metrics of JPEG2000+LDPC, Deep JSCC, VE-LDM, and EECD methods under different SNRs and channel states within DIV2K dataset.

under various channel conditions and noise levels. Specifically, the CBR for JPEG2000+LDPC is set at 0.05, while a unified CBR of 0.02 is employed for the other DL-based methods. Notably, the EECD method employs different subsequence lengths of $s=2$ and $s=1$ to validate its denoising proficiency. As illustrated in Fig. 9, a perceptual degradation in quality is observed for all methods in the low-SNR area, with a particularly pronounced decline under Rayleigh and Rician channels, likely induced by fading gains. Conventionally, joint compression and error correction methods exhibit slightly inferior performance compared to DL-based approaches across varying SNRs and channel types even with higher CBR. Furthermore, the VAE-based Deep JSCC method converges to a different perceptual quality level when compared to methods utilizing DMs and generator as SNR gradually increases. In

contrast, VE-LDM and EECD methods converge to the same level of perceptual quality in high-SNR area. Most importantly, the performance of EECD can be further approximated to that of the teacher model, i.e., VE-LDM, with increased resampling length, even in low-SNR area.

Analogously, experiments have been conducted within the DIV2K dataset, the results of which are depicted in Fig. 10. The CBR and CSI settings for the four methods are consistent with those utilized in the experiments for the AFHQ dataset. Specifically, the human-perceptual metrics for the denoising outcomes with the AWGN channel are superior to those with the Rayleigh and Rician channels. With regard to different channel denoising approaches, the original channel denoising DM undoubtedly achieved the most favorable performance, closely followed by the EECD curves with two different sub-sequence lengths, where the outcomes with $s=2$ were highly proximate to the denoising effects of the original VE-LDM, ensuring the normal transmission of semantic information.

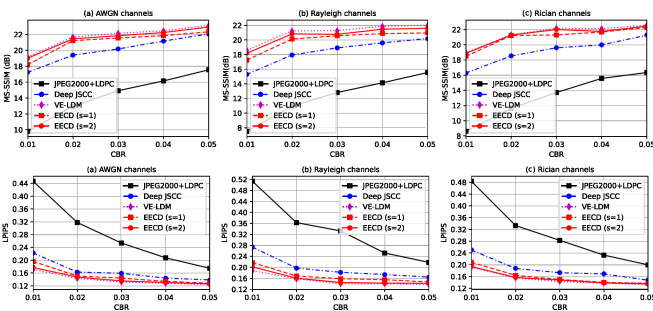


Fig. 11. Semantic metrics of JPEG2000+LDPC, Deep JSCC, VE-LDM, and EECD methods under different CBRs within AFHQ dataset.

Generally, an exemplary SemCom system is expected to maintain good reconstruction perceptual quality at a lower CBR, ultimately conserving communication bandwidth and reducing the communication burden. For different CBRs, Fig. 11 presents the changes in average perceptual metrics for the four different methods within the AFHQ dataset at CBRs ranging from 0.01 to 0.05. On one hand, the decoding quality of the conventional JPEG2000+LDPC method is heavily influenced by the compression ratio, with different CBRs potentially resulting in a manifold change in perceptual metrics. On the other hand, DL-based methods are less affected by CBR, indicating that DL-based models are robust and excel at extracting data features in the low-CBR area. Moreover, the channel denoising methods constructed based on DMs have attained superior performance under various CBR conditions.

E. Computational Complexity Analysis

Another paramount requirement for SemCom systems is low-latency communication, encompassing minimal data processing time for encoding, transmission, denoising, and decoding. The introduction of the EECD method enables the distillation of the multi-step denoising process in the latent space of the original DM into a few, or even a one-step sampling process, with only a slight perceptual quality trade-off, thus facilitating real-time SemCom. Specifically, since the VE-LDM and EECD methods both utilize the same robust

encoder and generator, only the computational complexity of the denoising process is analyzed. As discussed in [39], the noise prediction computational complexity for the denoising U-Net used by the DM is

$$\text{Time} \sim \mathcal{O} \left(\sum_{l=1}^L h_l^2 w_l^2 \cdot C_l \cdot C_{l-1} \cdot K_l^2 \right), \quad (32)$$

where L is the number of layers, $h_l w_l$ denotes the feature size and $h_l w_l \propto k$, C_l and C_{l-1} are the number of convolutional kernels in the l -th and $l-1$ -th layer, and K_l is the edge length of the convolutional kernel in the l -th layer. The channel denoising task requires only m NFE based on the noise level, hence the sampling computational complexity is $\text{Time} \sim m \times \mathcal{O} \left(\sum_{l=1}^L h_l^2 w_l^2 \cdot C_l \cdot C_{l-1} \cdot K_l^2 \right)$. As demonstrated by the time consumptions for different datasets under various CSI conditions in Table III, the computing time of VE-LDM may vary dramatically according to the noise level. However, after the application of EECD, where the denoising steps are fixed at the setting value ($s=2$), the overall time required for the encoding, denoising, and decoding sequence is substantially reduced to mere tens of milliseconds.

TABLE III
TIME CONSUMPTIONS OF VE-LDM AND EECD METHODS UNDER DIFFERENT CSIS AND DATASETS (VE-LDM/EECD (MILLISECONDS))

CSI	SNR (dB)	MNIST	AFHQ	DIV2K
AWGN	0	762.3/32.7	749.6/36.4	832.6/43.0
	10	543.5/33.0	513.6/36.3	591.3/43.2
	20	361.7/32.9	326.4/36.6	396.7/43.1
Rayleigh	0	762.7/32.5	750.1/36.5	833.1/43.1
	10	543.7/33.2	514.1/36.3	590.9/43.0
	20	362.3/33.0	327.8/36.8	397.1/43.3
Rician	0	761.9/32.5	749.7/36.4	832.8/43.2
	10	542.9/32.9	513.7/36.4	591.4/43.3
	20	362.1/32.4	327.0/36.5	396.9/43.1

Within the AFHQ dataset, the time consumption variability of VE-LDM and EECD models trained at different CBRs across an SNR range from 0dB to 20dB is illustrated in Fig. 12. In conjunction with the data presented in Table III and Fig. 12, it is evident that both the CBR and the image resolution can influence the channel denoising processing time. Consequently, VE-LDM may not meet the real-time denoising requirements in scenarios with low-SNR, high-CBR, or high-resolution. However, the predominant factor affecting the VE-LDM during the denoising process is the noise level. Consequently, in contrast to the VE-LDM's more substantial and variable time complexity during denoising, the proposed EECD method consistently maintains the time required for the denoising task within the scale of tens of milliseconds. Additionally, in line with the numerical results previously discussed, EECD does not significantly degrade semantic quality across various CSI scenarios.

VI. CONCLUSION

This paper introduces a wireless semantic communication (SemCom) system tailored to navigate the challenges of semantic ambiguities and channel noises. The proposed

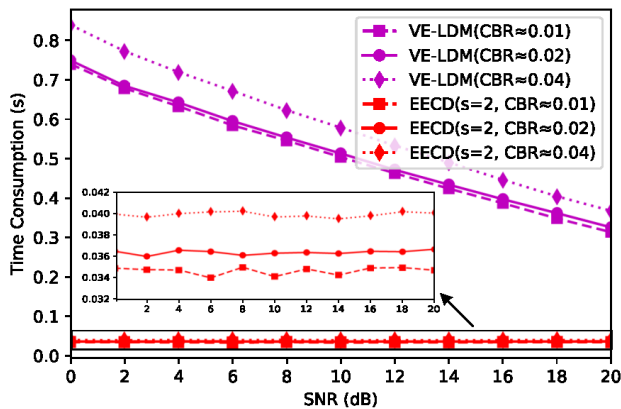


Fig. 12. Time consumptions of single image's encoding, denoising, and decoding process when utilizing VE-LDM and EECD methods under different CBRs and CSIs. SemCom system's proficiency in feature extraction diminishes the adverse effects of outliers in source data on deep learning-based communication systems and exhibits an impressive aptitude for rapid adaptation to data with unknown distribution, thereby augmenting the human-perceptual quality of decoded data. In the realm of data transmission, the advanced end-to-end consistency distillation (EECD) strategy facilitates real-time channel denoising across various pre-estimated channel state information (CSI) scenarios, achieving this with minimal perceptual quality degradation when contrasted with the existing channel denoising diffusion model techniques. Nonetheless, the real-time SemCom system based on diffusion models with unknown CSI and images with ultra-high resolution (2K/4K/6K) still warrants further investigation. Additionally, the integration of diffusion models into next-generation communication paradigms, specifically goal/task-oriented SemCom systems, poses an intriguing and significant topic for future exploration.

APPENDIX

A. Variational Upper Bound Transformation

Proof of Eq. (4):

$$\begin{aligned}
& \mathbb{E}_{q_\phi(z|\mathbf{x})} [-\log p_\psi(\mathbf{x}|z)] + \mathbb{E}_{q_\phi(z|\mathbf{x})} [\log q_\phi(z|\mathbf{x})] \\
&= \mathbb{E}_{q_\phi(z|\mathbf{x})} [-\log p_\psi(\mathbf{x}|z)] + \underbrace{\mathbb{E}_{q_\phi(z|\mathbf{x})} \left[\log \frac{q_\phi(z|\mathbf{x})}{p_\psi(z)} \right]}_{\mathbb{E}_q[\mathcal{D}_{KL}(q_\phi(z|\mathbf{x}) \| p_\psi(z))]} \\
&\quad + \mathbb{E}_{q_\phi(z|\mathbf{x})} [\log p_\psi(z)] \\
&\geq \mathbb{E}_{q_\phi(z|\mathbf{x})} \left[\log \frac{q_\phi(z|\mathbf{x})}{p_\psi(z)} - \log p_\psi(\mathbf{x}|z) \right] \\
&= \int q_\phi(z|\mathbf{x}) \log \frac{q_\phi(z|\mathbf{x})}{p_\psi(\mathbf{x}|z)p_\psi(z)} dz \\
&= \int q_\phi(z|\mathbf{x}) \left[\log p_\psi(\mathbf{x}) + \log \frac{q_\phi(z|\mathbf{x})}{p_\psi(z, \mathbf{x})} \right] dz - \mathbb{E}_q [\log p_\psi(\mathbf{x})] \\
&= \int q_\phi(z|\mathbf{x}) \left[\log \frac{q_\phi(z|\mathbf{x})}{p_\psi(z|\mathbf{x})} \right] dz + \mathbb{E}_q [-\log p_\psi(\mathbf{x})] \\
&= \mathbb{E}_{q(\mathbf{x})} [\mathcal{D}_{KL}(q_\phi(z|\mathbf{x}) \| p_\psi(z|\mathbf{x}))] + \mathbb{E}_{q_\psi(z)} [-\log p_\psi(\mathbf{x})]. \tag{33}
\end{aligned}$$

B. Proof of Robust Encoder's VUB

According to conditional Markov random field model [63], the joint distribution of data \mathbf{x} and data with semantic error $\mathbf{x} + \delta$ is

$$\begin{aligned}
& p_\psi(\mathbf{x}, \mathbf{x} + \delta) \propto \\
& \int p_\psi(\mathbf{x}|z) p_\psi(\mathbf{x} + \delta|z'') e^{-\frac{\beta}{2} d(z, z'')} p(z) p(z'') dz dz'', \tag{34}
\end{aligned}$$

where β denotes the nonnegative coupling parameter. Consequently, considering the joint distribution $q(z, z'')$, the evidence lower bound has the following form

$$\begin{aligned}
& \mathbb{E}_q [\log p_\psi(\mathbf{x}, \mathbf{x} + \delta)] \geq \mathbb{E}_{q(z)} [\log p_\psi(\mathbf{x}|z)] + \mathbb{E}_{q(z)} [\log p_\psi(z)] \\
& \quad + \mathbb{E}_{q(z'')} [\log p_\psi(\mathbf{x} + \delta|z'')] + \mathbb{E}_{q(z'')} [\log p_\psi(z'')] \\
& \quad - \frac{\beta}{2} \mathbb{E}_{q(z, z'')} d(z, z'') + \mathbb{E}_{q(z, z'')} [\log q(z, z'')]. \tag{35}
\end{aligned}$$

To decode clean data without changing the decoder parameters ψ , by simply integrating out $\mathbf{x} + \delta$ in Eq. (35) and according to Jensen's inequality, term $\mathbb{E}_q [-\log p_\psi(\mathbf{x})]$ can be transformed into Eq. (9).

REFERENCES

- [1] Y. Siriwardhana, P. Porambage, M. Liyanage, and M. Ylianttila, "A survey on mobile augmented reality with 5g mobile edge computing: Architectures, applications, and technical aspects," *IEEE Communications Surveys & Tutorials*, vol. 23, no. 2, pp. 1160–1192, 2021.
- [2] X. Huang, J. Riddell, and R. Xiao, "Virtual reality telepresence: 360-degree video streaming with edge-compute assisted static foveated compression," *IEEE Transactions on Visualization and Computer Graphics*, 2023.
- [3] F. E. Abrahamsen, Y. Ai, and M. Cheffena, "Communication technologies for smart grid: A comprehensive survey," *Sensors*, vol. 21, no. 23, p. 8087, 2021.
- [4] W. Wu, F. Zhou, B. Wang, Q. Wu, C. Dong, and R. Q. Hu, "Unmanned aerial vehicle swarm-enabled edge computing: Potentials, promising technologies, and challenges," *IEEE Wireless Communications*, vol. 29, no. 4, pp. 78–85, 2022.
- [5] M. Z. Chowdhury, M. Shahjalal, S. Ahmed, and Y. M. Jang, "6g wireless communication systems: Applications, requirements, technologies, challenges, and research directions," *IEEE Open Journal of the Communications Society*, vol. 1, pp. 957–975, 2020.
- [6] E. Boursoulatzé, D. Burth Kurka, and D. Gündüz, "Deep joint source-channel coding for wireless image transmission," *IEEE Transactions on Cognitive Communications and Networking*, vol. 5, no. 3, pp. 567–579, 2019.
- [7] J. Xu, T.-Y. Tung, B. Ai, W. Chen, Y. Sun, and D. D. Gündüz, "Deep joint source-channel coding for semantic communications," *IEEE Communications Magazine*, vol. 61, no. 11, pp. 42–48, 2023.
- [8] G. Ginesu, M. Pintus, and D. D. Giusto, "Objective assessment of the webp image coding algorithm," *Signal processing: image communication*, vol. 27, no. 8, pp. 867–874, 2012.
- [9] G. K. Wallace, "The jpeg still picture compression standard," *IEEE transactions on consumer electronics*, vol. 38, no. 1, pp. xviii–xxxiv, 1992.
- [10] C. Christopoulos, A. Skodras, and T. Ebrahimi, "The jpeg2000 still image coding system: an overview," *IEEE transactions on consumer electronics*, vol. 46, no. 4, pp. 1103–1127, 2000.
- [11] Y. Fan, J. Yu, and T. S. Huang, "Wide-activated deep residual networks based restoration for bpg-compressed images," in *Proceedings of the IEEE conference on computer vision and pattern recognition Workshops*, 2018, pp. 2621–2624.
- [12] W. Yang *et al.*, "Semantic communications for future internet: Fundamentals, applications, and challenges," *IEEE Communications Surveys & Tutorials*, vol. 25, no. 1, pp. 213–250, 2022.
- [13] X. Luo, H.-H. Chen, and Q. Guo, "Semantic communications: Overview, open issues, and future research directions," *IEEE Wireless Communications*, vol. 29, no. 1, pp. 210–219, 2022.
- [14] H. Xie, Z. Qin, G. Y. Li, and B.-H. Juang, "Deep learning enabled semantic communication systems," *IEEE Transactions on Signal Processing*, vol. 69, pp. 2663–2675, 2021.

- [15] J. Dai *et al.*, “Nonlinear transform source-channel coding for semantic communications,” *IEEE Journal on Selected Areas in Communications*, vol. 40, no. 8, pp. 2300–2316, 2022.
- [16] K. He, X. Zhang, S. Ren, and J. Sun, “Deep residual learning for image recognition,” in *Proceedings of the IEEE conference on computer vision and pattern recognition*, 2016, pp. 770–778.
- [17] J. Xu, B. Ai, W. Chen, A. Yang, P. Sun, and M. Rodrigues, “Wireless image transmission using deep source channel coding with attention modules,” *IEEE Transactions on Circuits and Systems for Video Technology*, vol. 32, no. 4, pp. 2315–2328, 2021.
- [18] N. Farsad, M. Rao, and A. Goldsmith, “Deep learning for joint source-channel coding of text,” in *2018 IEEE international conference on acoustics, speech and signal processing (ICASSP)*. IEEE, 2018, pp. 2326–2330.
- [19] H. Zhang, S. Shao, M. Tao, X. Bi, and K. B. Letaief, “Deep learning-enabled semantic communication systems with task-unaware transmitter and dynamic data,” *IEEE Journal on Selected Areas in Communications*, vol. 41, no. 1, pp. 170–185, 2022.
- [20] D. Huang, F. Gao, X. Tao, Q. Du, and J. Lu, “Toward semantic communications: Deep learning-based image semantic coding,” *IEEE Journal on Selected Areas in Communications*, vol. 41, no. 1, pp. 55–71, 2022.
- [21] Z. Weng and Z. Qin, “Semantic communication systems for speech transmission,” *IEEE Journal on Selected Areas in Communications*, vol. 39, no. 8, pp. 2434–2444, 2021.
- [22] H. Xie, Z. Qin, X. Tao, and K. B. Letaief, “Task-oriented multi-user semantic communications,” *IEEE Journal on Selected Areas in Communications*, vol. 40, no. 9, pp. 2584–2597, 2022.
- [23] J. Ho, A. Jain, and P. Abbeel, “Denoising diffusion probabilistic models,” *Advances in neural information processing systems*, vol. 33, pp. 6840–6851, 2020.
- [24] J. Song, C. Meng, and S. Ermon, “Denoising diffusion implicit models,” *arXiv preprint arXiv:2010.02502*, 2020.
- [25] H. Du *et al.*, “Beyond deep reinforcement learning: A tutorial on generative diffusion models in network optimization,” *arXiv preprint arXiv:2308.05384*, 2023.
- [26] H. Du, J. Wang, D. Niyato, J. Kang, Z. Xiong, and D. I. Kim, “AI-generated incentive mechanism and full-duplex semantic communications for information sharing,” *IEEE Journal on Selected Areas in Communications*, 2023.
- [27] J. Chen, D. You, D. Gündüz, and P. L. Dragotti, “Commin: Semantic image communications as an inverse problem with inn-guided diffusion models,” in *ICASSP 2024-2024 IEEE International Conference on Acoustics, Speech and Signal Processing (ICASSP)*. IEEE, 2024, pp. 6675–6679.
- [28] E. Grassucci, S. Barbarossa, and D. Comminiello, “Generative semantic communication: Diffusion models beyond bit recovery,” *arXiv preprint arXiv:2306.04321*, 2023.
- [29] S. F. Yilmaz, X. Niu, B. Bai, W. Han, L. Deng, and D. Gunduz, “High perceptual quality wireless image delivery with denoising diffusion models,” *arXiv preprint arXiv:2309.15889*, 2023.
- [30] M. Yang, D. Gao, F. Xie, J. Li, X. Song, and G. Shi, “Sg2sc: A generative semantic communication framework for scene understanding-oriented image transmission,” in *ICASSP 2024-2024 IEEE International Conference on Acoustics, Speech and Signal Processing (ICASSP)*. IEEE, 2024, pp. 13 486–13 490.
- [31] Y. Choukroun and L. Wolf, “Denoising diffusion error correction codes,” *arXiv preprint arXiv:2209.13533*, 2022.
- [32] N. Zilberstein, A. Swami, and S. Segarra, “Joint channel estimation and data detection in massive mimo systems based on diffusion models,” in *ICASSP 2024-2024 IEEE International Conference on Acoustics, Speech and Signal Processing (ICASSP)*. IEEE, 2024, pp. 13 291–13 295.
- [33] F. Jiang *et al.*, “Large generative model assisted 3d semantic communication,” *arXiv preprint arXiv:2403.05783*, 2024.
- [34] Z. Jiang, X. Liu, G. Yang, W. Li, A. Li, and G. Wang, “Diffsc: Semantic communication framework with enhanced denoising through diffusion probabilistic models,” in *ICASSP 2024-2024 IEEE International Conference on Acoustics, Speech and Signal Processing (ICASSP)*. IEEE, 2024, pp. 13 071–13 075.
- [35] E. Grassucci, C. Marinoni, A. Rodriguez, and D. Comminiello, “Diffusion models for audio semantic communication,” in *ICASSP 2024-2024 IEEE International Conference on Acoustics, Speech and Signal Processing (ICASSP)*. IEEE, 2024, pp. 13 136–13 140.
- [36] H. Du *et al.*, “Exploring collaborative distributed diffusion-based ai-generated content (aigc) in wireless networks,” *IEEE Network*, 2023.
- [37] T. Wu *et al.*, “Cddm: Channel denoising diffusion models for wireless semantic communications,” *IEEE Transactions on Wireless Communications*, pp. 1–1, 2024.
- [38] M. Kim, R. Fritschek, and R. F. Schaefer, “Learning end-to-end channel coding with diffusion models,” in *WSA & SCC 2023; 26th International ITG Workshop on Smart Antennas and 13th Conference on Systems, Communications, and Coding*, 2023, pp. 1–13.
- [39] J. Pei, J. Wang, D. Shi, and P. Wang, “Detection and imputation based two-stage denoising diffusion power system measurement recovery under cyber-physical uncertainties,” *IEEE Transactions on Smart Grid*, pp. 1–1, 2024.
- [40] D. Adesina, C.-C. Hsieh, Y. E. Sagduyu, and L. Qian, “Adversarial machine learning in wireless communications using rf data: A review,” *IEEE Communications Surveys & Tutorials*, vol. 25, no. 1, pp. 77–100, 2022.
- [41] G. Zhang, Q. Hu, Z. Qin, Y. Cai, and G. Yu, “A unified multi-task semantic communication system with domain adaptation,” in *GLOBECOM 2022-2022 IEEE Global Communications Conference*. IEEE, 2022, pp. 3971–3976.
- [42] J. Adler and S. Lunz, “Banach wasserstein gan,” *Advances in neural information processing systems*, vol. 31, 2018.
- [43] Y. Song, P. Dhariwal, M. Chen, and I. Sutskever, “Consistency models,” *arXiv preprint arXiv:2303.01469*, 2023.
- [44] A. Vahdat, K. Kreis, and J. Kautz, “Score-based generative modeling in latent space,” *Advances in neural information processing systems*, vol. 34, pp. 11 287–11 302, 2021.
- [45] R. Rombach, A. Blattmann, D. Lorenz, P. Esser, and B. Ommer, “High-resolution image synthesis with latent diffusion models,” in *Proceedings of the IEEE/CVF conference on computer vision and pattern recognition*, 2022, pp. 10 684–10 695.
- [46] G. Zheng *et al.*, “Mobility-aware split-federated with transfer learning for vehicular semantic communication networks,” *IEEE Internet of Things Journal*, pp. 1–1, 2024.
- [47] R. Abdal, Y. Qin, and P. Wonka, “Image2stylegan: How to embed images into the stylegan latent space?” in *Proceedings of the IEEE/CVF international conference on computer vision*, 2019, pp. 4432–4441.
- [48] Z. Wang, H. Zheng, P. He, W. Chen, and M. Zhou, “Diffusion-gan: Training gans with diffusion,” *arXiv preprint arXiv:2206.02262*, 2022.
- [49] W. Luo, T. Hu, S. Zhang, J. Sun, Z. Li, and Z. Zhang, “Diff-instruct: A universal approach for transferring knowledge from pre-trained diffusion models,” *Advances in Neural Information Processing Systems*, vol. 36, 2024.
- [50] W. Xia, Y. Zhang, Y. Yang, J.-H. Xue, B. Zhou, and M.-H. Yang, “Gan inversion: A survey,” *IEEE transactions on pattern analysis and machine intelligence*, vol. 45, no. 3, pp. 3121–3138, 2022.
- [51] A. B. L. Larsen, S. K. Sønderby, H. Larochelle, and O. Winther, “Autoencoding beyond pixels using a learned similarity metric,” in *International conference on machine learning*. PMLR, 2016, pp. 1558–1566.
- [52] R. B. Lanfredi, J. D. Schroeder, and T. Tasdizen, “Quantifying the preferential direction of the model gradient in adversarial training with projected gradient descent,” *Pattern Recognition*, vol. 139, p. 109430, 2023.
- [53] T. Cemgil, S. Ghaisas, K. D. Dvijotham, and P. Kohli, “Adversarially robust representations with smooth encoders,” in *International Conference on Learning Representations*, 2019.
- [54] T. Karras, M. Aittala, T. Aila, and S. Laine, “Elucidating the design space of diffusion-based generative models,” *Advances in Neural Information Processing Systems*, vol. 35, pp. 26 565–26 577, 2022.
- [55] Z. Zhou, D. Chen, C. Wang, and C. Chen, “Fast ode-based sampling for diffusion models in around 5 steps,” *arXiv preprint arXiv:2312.00094*, 2023.
- [56] F. Bao, C. Li, J. Sun, J. Zhu, and B. Zhang, “Estimating the optimal covariance with imperfect mean in diffusion probabilistic models,” *arXiv preprint arXiv:2206.07309*, 2022.
- [57] C. Lu, Y. Zhou, F. Bao, J. Chen, C. Li, and J. Zhu, “Dpm-solver++: Fast solver for guided sampling of diffusion probabilistic models,” *arXiv preprint arXiv:2211.01095*, 2022.
- [58] T. Huang *et al.*, “Knowledge diffusion for distillation,” *Advances in Neural Information Processing Systems*, vol. 36, 2024.
- [59] R. Zhang, P. Isola, A. A. Efros, E. Shechtman, and O. Wang, “The unreasonable effectiveness of deep features as a perceptual metric,” in *Proceedings of the IEEE conference on computer vision and pattern recognition*, 2018, pp. 586–595.
- [60] Y. Choi, Y. Uh, J. Yoo, and J.-W. Ha, “Stargan v2: Diverse image synthesis for multiple domains,” in *Proceedings of the IEEE/CVF*

conference on computer vision and pattern recognition, 2020, pp. 8188–8197.

- [61] R. Timofte *et al.*, “Ntire 2018 challenge on single image super-resolution: Methods and results,” in *The IEEE Conference on Computer Vision and Pattern Recognition (CVPR) Workshops*, June 2018.
- [62] J. Chen, A. Dholakia, E. Eleftheriou, M. P. Fossorier, and X.-Y. Hu, “Reduced-complexity decoding of ldpc codes,” *IEEE transactions on communications*, vol. 53, no. 8, pp. 1288–1299, 2005.
- [63] C. Sutton, A. McCallum *et al.*, “An introduction to conditional random fields,” *Foundations and Trends® in Machine Learning*, vol. 4, no. 4, pp. 267–373, 2012.